SI Appendix

Material and methods

Sedimentology

Four sections of the Xujiachong Formation were examined at: Xujiachong, Xiaoguankou, Longhua, and Baojia Tunnel (Fig. 1*C*). Red mudstones (paleosols) with plant traces are recognized within these sections, where abundant *Drepanophycus* remains have been observed by the present authors or have been previously reported (1, 2). In the Xujiachong section, the logged descriptions of the Xujiachong Formation (3) were re-examined, and most of their observations, confirmed. The Xujiachong Formation in the Xiaoguankou section was newly measured and logged. The lithological columns of several beds at Xujiachong and Xiaoguankou are presented in Figure 2. The Longhua section, where *Drepanophycus* was first reported from South China (1), includes paleosols with plant traces similar to those in other sections. The Baojia Tunnel section is located within a railway tunnel under construction (Aug.–Oct., 2014), and it is not possible to approach the outcrops. However, freshly excavated rocks were stacked nearby, enabling us to observe the sedimentological features from a three-dimensional perspective.

In order to obtain paleoenvironmental and geomorphological information for vegetation development within the Xujiachong Formation, outcrops and sequences were observed in detail, including primary sedimentary structures, bed geometries, thicknesses, grading, contacts, and repetition cycles (Figs. S1−S9; Table S1). Hand specimens of different sedimentological facies were collected for thin-section petrological analysis. Five lithological facies are recognized,

including: gray intraformational conglomerate (Gt); medium to thickly bedded gray sandstone (St); thinly bedded gray-green sandstone (Spr); gray-green mudstone and siltstone (Fg); and red pedified mudstone (Frp). The facies associations indicate a fluvial environment for the Xujiachong Formation, broadly consistent with previous interpretations (3). Detailed sedimentological analysis demands much additional work and discussion, and therefore has not been addressed in this paper.

To reveal the density of plant traces in paleosols, we selected bedding surfaces at Xujiachong that clearly show transections of plant traces. Quadrats (100 mm by 100 mm for each) on bedding surfaces were used to estimate the number of traces per unit area (Fig. S8 *D* and *E*; Table S2). To visualize the trace distribution pattern on a bedding surface (Fig. S8*E*), firstly, the x and y coordinates of traces on the selected bedding surface were obtained from the digitized illustration by using the software tpsDig (4); the coordinates were then loaded into the software PAST, in which was plotted a Kernel density map of traces (5). The coordinate scores were analyzed for point pattern in PAST, by using nearest-neighbour analysis to test for clustering or overdispersion of trace transections on the bedding surface (5). A ca. 2000-cm^3 rock block collected from Xiaoguankou (sample 1410XGK37) was transversely sectioned with an interval of ca. 2 cm, and representative sections and side views of the rock block, as well as a reconstruction of the three-dimensional pattern of rhizome traces within the rock matrix (produced in the software 3d Max), were illustrated in Fig. S10−11.

Fresh whole-rock samples were collected from the Xiaoguankou section and Cycles 33−37 of the Xujiachong section for geochemical analyses (see below). Carbonate nodules in paleosols were collected from the Xiaoguankou and Xujiachong sections, and isolated from the rock matrix for measurement of sizes (Table S3), and stable carbon and oxygen isotopic analyses.

Palaeobotany

Numerous remains (preserved as compressions and impressions) of *Drepanophycus*,

Zosterophyllum, and other plants were collected from the four sections. The beds containing plant remains were recorded (Fig. 2). To reveal the details of axial branching and lateral appendages, preparations with steel needles were made on some selected specimens under a binocular dissecting microscope. Close attention was devoted to comparisons between the compression remains and the plant traces preserved in sediments, including their width, branchings, extensions, and lateral appendages (leaves) if present. Most remains of *Drepanophycus* can be assigned to *D. qujingensis* Li et Edwards (Fig. S6 *C*−*H*).

Geochemical measurements

Twenty-four whole-rock samples from Xujiachong (Cycles 33−37) and 17 samples from Xiaoguankou were investigated for elemental analysis. Major and minor oxide contents (SiO_2, Al_2O_3, Fe_2O_3, CaO, MgO, K_2O, Na_2O, MnO, TiO_2, and P_2O_5) were determined with a Thermo ARL ADVANTXP+ sequential X-ray fluorescence (XRF) spectrometer at the Key Laboratory of Orogenic Belts and Crustal Evolution, Peking University. Samples were milled to 200 mesh fine powder. After pretreatment in a drying oven for 4 h at 105°C, the powders were then fused in glass disks (0.4 g of dried sample and 4 g of lithium metaborate + tetraborate flux in a platinum crucible) using an automated fusion machine. The reliability of analytical results was checked by duplicate analyses of a few investigated samples and two geological reference materials (GSR-4, GSR-8). Precision values were: 0.6% for SiO_2; 0.3% for Al_2O_3; 1.0% for Fe_2O_3 (total); 0.9% for CaO; 0.8% for MgO, MnO and TiO2; 1.3% for K_2O; 2.4% for Na_2O; and 2.1% for P_2O_5.

Trace element contents (Ba, Sr and REEs) of 31 samples (15 from Xujiachong and 16 from Xiaoguankou) were measured using an Agilent 7500Ce ICP-MS instrument at the Key Laboratory of Orogenic Belts and Crustal Evolution, Peking University. Samples were milled to 200 mesh fine powder, and were dried in a drying oven for 2 h at 105°C. For acid digestion, 25 mg of dried samples were heated with 1.5 ml concentrated HNO_3 + 1.5 ml concentrated HF in closed Teflon dissolution bottles. Next, the acids were evaporated to dryness and residues were

evaporated with 1.5 ml HNO_3 (1:1 HNO_3 and H_2O by v/v), 1.5 ml HF, and $HClO_4$. The dried samples were then heated with 3 ml HNO_3 (1:1 HNO_3 and H_2O solution) in closed bottles, next dried, and again heated with 1 ml HNO_3 until clear solutions were obtained. For ICP-MS analysis the solutions were diluted to 1:2000. The analytical procedure was controlled by using three geological standard materials (GSR-1, GSR-4 and GSR-5) and a few randomly selected samples that were measured in parallel. Analytical precision values were 4% for Ba, 5% for Sr, and generally better than 7% for REEs.

Major and minor oxides data are presented in weight percentage (wt%) and trace elements in parts per million (ppm) (Tables S4, S5). When calculating molecular weathering ratios, the raw abundances were converted into moles by dividing the weight percentage (or ppm) by the molecular mass.

Compositional X-ray maps of the paleosol samples (Fig. S12) were obtained using Energy Dispersive Spectrometry (Oxford INCA Energy 350) attached to an FEI Quanta-650 FEG scanning electron microscope, at the Key Laboratory of Orogenic Belts and Crustal Evolution at Peking University. The working condition is with an acceleration voltage of 20 kV, a beam current of 2.5-3.0 nA (spot 5.5), and a working distance of 10 mm.

Twenty-nine samples of carbonate nodules recovered from paleosols (17 from Xujiachong and 12 from Xiaoguankou) were analyzed for stable carbon and oxygen isotopes (Table S6). Micrites of the nodules were further sampled by using a dental drill under a light microscope. Twenty-nine whole-rock samples from the same horizons as the carbonate nodules, plus two additional samples from adjacent horizons (gray-green siltstone; 148XJC019, 1410XGK22), were analyzed for carbon isotopes of organic matter (Table S6).

Carbonate nodule samples were analyzed for stable carbon isotopes ($\delta^{13}C_{carb}$) and oxygen isotopes ($\delta^{18}O_{carb}$) at Nanjing Institute of Geology and Palaeontology, Chinese Academy of Sciences. An aliquot of 100 to 150 μg of each sample was reacted with phosphoric acid (H_3PO_4) for 150−200 s at 72°C in a Kiel IV carbonate device connected to a MAT 253 mass spectrometer. Precision for the analyses was better than 0.03‰ for $\delta^{13}C$ and 0.08‰ for $\delta^{18}O$.

The Chinese Standard Material GBW-04405 was used as a working standard, with the $\delta^{13}C_{carb}$ value of 0.57‰ ± 0.03‰ and the $\delta^{18}O$ value of −8.49‰ ± 0.13‰. All data are presented in standard per mil (‰) notation relative to Vienna Pee Dee Belemnite (V-PDB).

For organic carbon isotope ($\delta^{13}C_{organic\ matter}$ or simply as $\delta^{13}C_{OM}$) analysis, ca. 20 g of each powdered sample (TOC contents generally less than 1%) were put into 500 ml polypropylene beakers to react with 50−100 ml of 10% v/v HCl for one night. After removal of the supernatant, the residues were reacted with 50−100 ml of 40% v/v HF for three days, and then washed with distilled water to neutrality. In order to remove carbonates completely, the residues were then heated with 50−100 ml 15% v/v HCl, at 200°C for 20 minutes, and washed with distilled water to neutrality. The obtained powders were analyzed with a Flash EA 2000 coupled with Thermo Scientific™ DELTA V isotope ratio mass spectrometer. Analyses were carried out at Nanjing Institute of Geology and Palaeontology. All results are given in the standard delta notation as per mil difference to the Vienna Pee Dee Belemnite (V-PDB). The analytical precision was better than 0.15‰. The working standard materials are GBW04407, with a $\delta^{13}C$ value of −22.43‰ ± 0.07‰ and IVA 33802174, with a $\delta^{13}C$ value of −40.81‰ ± 0.17‰.

Detailed description of plant traces

Plant traces were found in various lithofacies. The most common type of trace is 5.9−18 mm wide (average 10.5 mm; n = 90) and is interpreted as rhizome traces of *Drepanophycus* (see text). The second type is much thinner and occurs only occasionally (Figs. S4 *G* and *H*, and S6 *A* and *B*, arrows), and is 2.2−3.2 mm wide and at least 57 mm long. Some of these thinner traces have been found attached to the rhizome traces (Fig. S6*B*), and some show dichotomous branching (Fig. S4*H*, lower arrow). We interpret this second type as traces of adventitious roots of *Drepanophycus*, in that they are attached to the rhizome traces and that their size is comparable to the adventitious roots of *Drepanophycus*, as described by previous authors (1, 6−8).

Rhizome traces of *Drepanophycus*:

The plant rhizome traces are characterized by multiple K- or H-shaped branchings and thus demonstrate a complex network-like structure both in vertical and horizontal directions. Typically, a parent rhizome divides to produce a lateral branch at nearly 90º, and after a short distance, this lateral trace divides to produce two daughter traces which diverge at a wide angle (K-shaped) to almost 180º (H-shaped); during this process, the trace width changes little (Fig. S4 *F*–*H*). In vertical sections, one of the daughter traces is downwardly directed, and the other, upwardly directed (Fig. S13). The interval between branching points varies from 10.9 to 90.5 mm (n = 20). The longest measurable, continuous trace reaches over 3 m vertically.

One sample shows that a horizontally extended trace divides at least six times within a ca. 100-mm length, forming three upwardly directed branches and three downwardly ones (Figs. S8*B* and S13*B*), and the vertical branches further divide after a short distance. In vertical sections of rock, the branching of the traces appears more frequent at some horizontal levels than at others (Figs. S8*B* and S13, arrows). The vertical distance between such levels is ca. 80 mm, probably indicating the rhythmic growth of the plant. On bedding surfaces, some traces are shown as horizontal extensions (Figs. S4*H*, S6*A* and S8*C*), with similarly complex branching as on vertical sections. Thus, horizontal and vertical extensions of traces with repeated H- or K-shaped branching form complex network-like structures in the matrix (Figs. 2*H*–*J* and S13).

On vertical section, the traces are typically shown as rhizohaloes, filled with clays finer than or similar to the matrix. The transections of traces, showing on bedding surfaces, are oval or circular in shape (Figs. 2*J*, and S8 *C* and *D*). The traces show a two-layered structure in transection, with the inner layer finer (argillaceous) in grain size (Fig. S9*F*).

Sandstones underlying paleosols also may contain vertical and horizontal traces (Fig. S4 *C*–*E*), although less abundantly. Horizontal traces commonly occur in the bottom beds of a cycle, which truncate the underlying fines of the previous cycle which may preserve extensive traces (Fig. S5*F*). Plant traces and compression remains typical of *Drepanophycus* can be found crosscutting sandstone bedding, indicating *in situ* burial (Fig. S4 *B*–*E*).

Quantifying the erosion-reducing potential of *Drepanophycus* rhizomes

Quantifying the effects of plant roots in reducing soil erosion is difficult because of the diversity of plant root architectures and soil structures, although such effects are manifest to people with experience in stabilizing agricultural fields, slopes, and roadsides. For assessing the erosion-reducing potential of *Drepanophycus* rhizomes, it is necessary to rely upon comparative studies between fossil and modern plants. For modern plants, Vannoppen et al. (9) have presented a state-of-the-art review on this issue: they compiled a global dataset of measured soil detachment ratios (SDR, see below) due to concentrated flow (flood) and root properties such as root density (RD) and root length density (RLD); and they then found that the SDR can be described by a non-linear regression function of RD and RLD. Some of their main points are summarized below:

(i) The soil detachment ratio (SDR) due to concentrated flow is the ratio between the absolute soil detachment rate (ASD) for a soil sample with roots and the ASD for a corresponding soil sample without roots, i.e. the reference value. Thus, there is no erosion reduction when SDR = 1, while the erosion is almost completely reduced when SDR = 0. Various root properties, such as root diameter, rooting depth, root architecture, root tensile strength, root density (RD), root length density (RLD), are all associated with their mechanical effects in soil. However, Vannoppen et al. (9) suggested that the root length density (RLD) is a much more suitable proxy for SDR compared to RD and other variables. The RLD means the total length of plant roots in a certain volume of soil.

(ii) The observed RLD for modern plants ranges from 0.35 km/m^3 to more than 6000 km/m^3, based on the compilation of 274 observations from six empirical studies (9). For these 274 observations, there is a non-linear regression function between RLD and SDR:

$$SDR = RLD^{-0.46}/(0.56 + RLD^{-0.46})$$ (n = 274, including both fibrous and tap roots)

(Equation 1) (9)

As suggested by Vannoppen et al. (9), this model explains only a limited amount of the large variance in the dataset (with a low model efficiency). However, it can be used to predict a general trend in the data.

To refine the above model, the soil textures and root architectures were also taken into account, resulting in the following function, with a significant improvement of model efficiency:

$$SDR = RLD^{-0.94}/(0.20 + RLD^{-0.94})\ (n = 109;\ \text{fibrous roots, non-sandy soils})$$

(Equation 2) (9)

The modeling study for modern plant roots forms the basis for our estimate of the likely mechanical effects of *Drepanophycus* rhizomes. We suggest that the total length of *Drepanophycus* rhizomes per unit of sediment can be directly compared with the RLD of modern plants. The RLD of *Drepanophycus* rhizomes can be estimated to be 0.8−1.3 km/m^3 (Table S7 note; Figs. S10 and S11), a value at the lower end of the range for modern plant roots (9). The rhizomes of *Drepanophycus* are dissimilar to tap root systems, which have a main root and small laterals, and are also dissimilar to fibrous root systems, which are characterized by numerous fine roots (e.g. < 2 mm in diameter). However, *Drepanophycus* rhizomes may be considered intermediate between these two extremes, although they are more comparable to fibrous root systems in that they do not show a hierarchy pattern with a central main rhizome and several lateral smaller roots, but their width usually keeps constant over a considerable length.

Here, we use both Equation 1 (for both fibrous and tap roots) and Equation 2 (for fibrous roots and non-sandy soils) to estimate the potential effects of *Drepanophycus* rhizomes in reducing soil erosion. Given that the RLD is 0.8−1.3 km/m^3, the estimated SDR values range from 0.61 to 0.86, indicating a weak to modest reduction of soil erosion by *Drepanophycus* rhizomes (Table S8).

Uncertainty for such an estimation comes from two sources. Firstly, comparability of *Drepanophycus* rhizomes to modern plant roots may be unclear. The empirical studies of root/rhizome effects have been largely based on modern angiosperms (9). Nevertheless, *Drepanophycus* rhizomes and the fibrous root systems of modern herbs are similar in that the xylem strands of *Drepanophycus* rhizomes, which are usually 1−2 mm wide (1), and are comparable in size to the fine roots of modern plants, while the wide parenchymatous cortex may have been mechanically irrelevant. Secondly, it should be noted that empirical studies of modern plant roots mainly focused on their short-term, mechanical effects (few studies evaluated root permeated soil samples older than a few months) (9). For *Drepanophycus* rhizomes, however, other processes should also be taken into account: for instance, the decomposition of rhizomes is an important source of organic matter, which would increase the soil structure, and, in some cases, contribute to formation of rhizocretions (Fig. S10 *B* and *D*) to provide additional resistance against erosion.

Fig. S1. Facies Gt – conglomerate. Facies codes (same in Figs. S1−S9): gray intraformational conglomerate (Gt); medium to thickly bedded gray sandstone (St); thinly bedded gray-green sandstone (Spr); gray-green mudstone and siltstone (Fg); and red pedified mudstone (Frp). Scale (same in Figs. S1−S9): the coin is 20 mm in diameter; the marker pen is 140 mm in length; and the hammer is 280 mm in length. If not indicated, the outcrops in Figs. S1−S9 are all from the Xujiachong section. (*A*) Field outcrop showing basal conglomerate of Cycle 66. Scale bar, 40 mm. (*B*−*D*) Rocks from the Baojia Tunnel section. (*B*) Vertical section of conglomerate with clasts, and fining upwards to coarse sandstone. (*C*) Bedding surface of conglomerate. (*D*) Polished vertical section of conglomerate showing moderately sorted mud clasts. Scale bar, 10 mm.

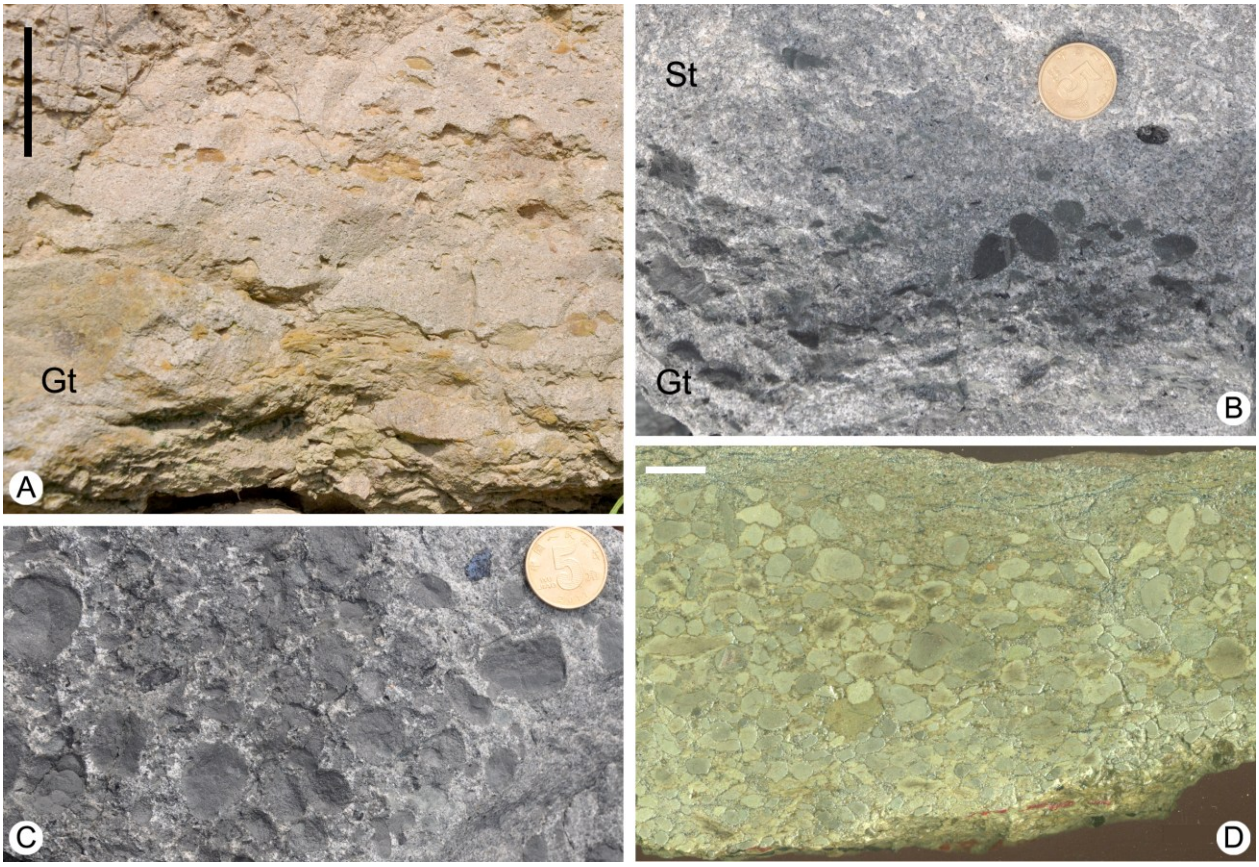

Fig. S2. Field outcrop of the Xujiachong Formation in the Xujiachong section. Facies codes: medium to thickly bedded gray sandstone (St); thinly bedded gray-green sandstone (Spr); gray-green mudstone and siltstone (Fg); and red pedified mudstone (Frp). (*A*) Cycle 78, medium to thickly bedded sandstone (St), showing channel form and lenticular geometries of sandstones. (*B*) Lithological cycles, from the top of Cycle 66 to Cycle 68. Basal sandstone of Cycle 68 is enlarged in Fig. S3*F*. (*C*) Cycle 54, heterolithic facies, showing couplets of thinly bedded fine-grained sandstone (Spr) and gray-green siltstone (Fg).

Fig. S2.

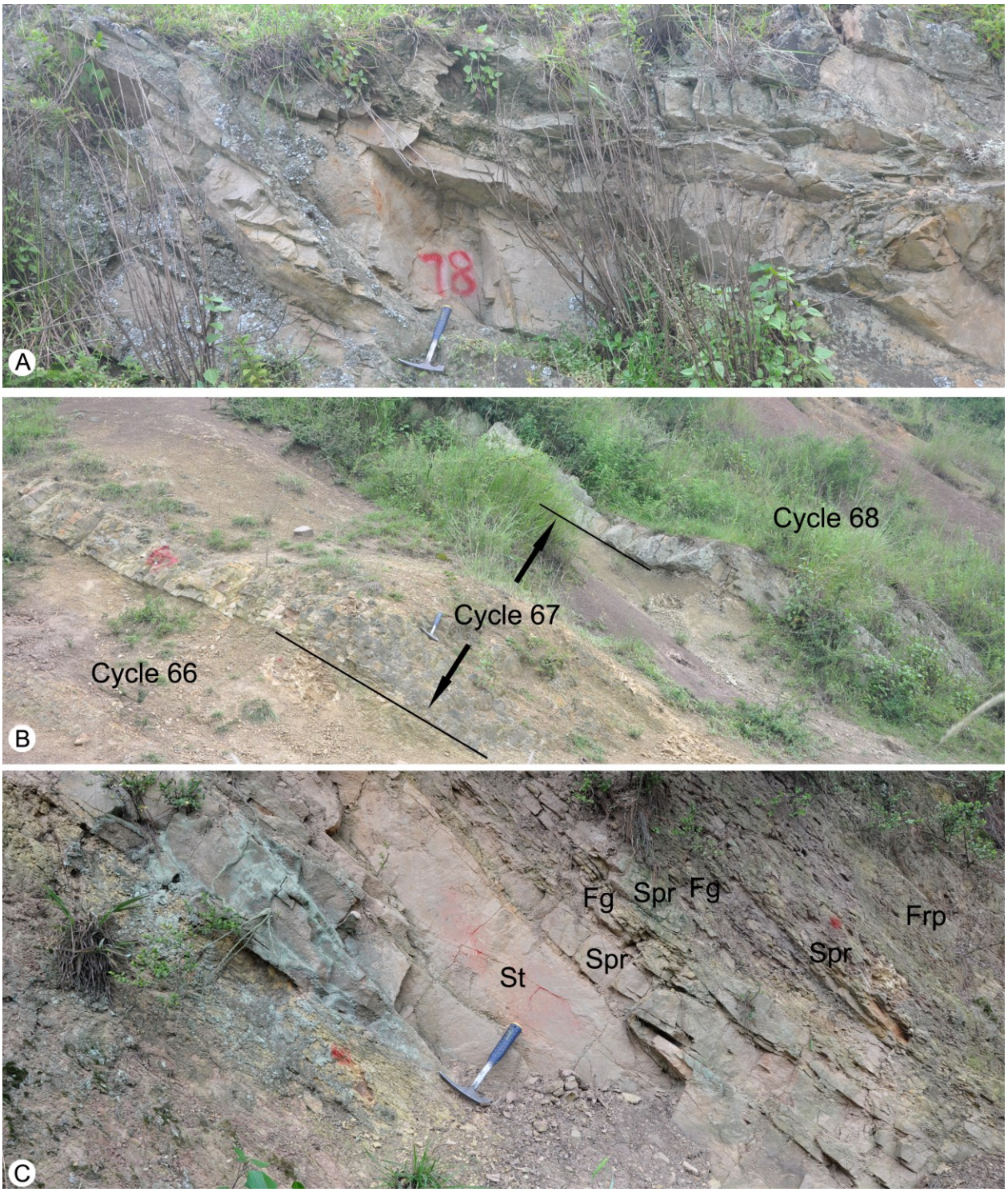

Fig. S3. Facies St – medium to thickly bedded sandstone. (*A*) Cycle 58, trough cross-bedding. (*B*) Cycle 75, showing truncation of lenticular sandstone bodies and lens of green siltstone (arrow). (*C*) Cycle 58, tabular cross-bedding. (*D*) Cycle 89, tabular cross-bedding. (*E*) Cycle 89, trough cross-bedding. (*F*) Cycle 68, with an erosional base.

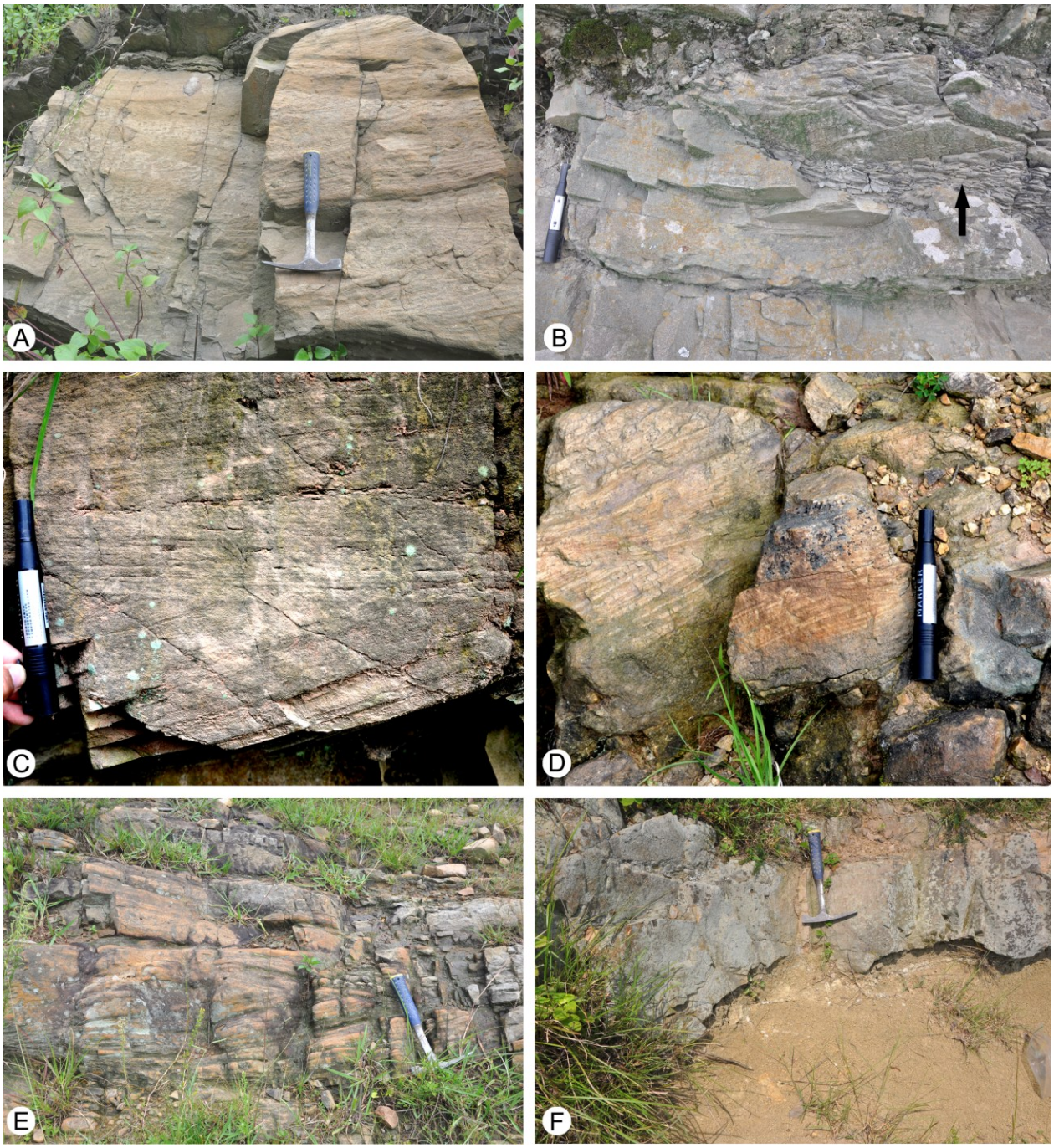

Fig. S4. Field outcrop, and plant remains and traces of the Xujiachong Formation. (*A*) Cycle 66, couplets of thinly bedded, lenticular sandstone (Facies Spr) and siltstone (Facies Fg), overlain by thick siltstone and then by red mudstone (paleosols, Facies Frp). (*B*−*H*) Specimens from the Baojia Tunnel section. (*B*) Vertical aerial axes of *Drepanophycus qujingensis in situ* preserved in sandstone with planar bedding. Scale bar, 20 mm. (*C*) Vertical plant traces (arrows) in thinly bedded sandstone. (*D*) Vertical plant traces in sandstone. Arrow points a broken level, where the bedding surface is shown in (*E*). Scale bar, 20 mm. (*E*) Traces on bedding surface, showing vestige of *Drepanophycus* axes with leaves (arrow). Scale bar, 10 mm. (*F*) Vertical plant traces in coarse siltstone, showing complex branching pattern. Scale bar, 20 mm. (*G*, *H*) Traces of rhizomes and thin, adventitious roots (arrows). Scale bars, 20 mm.

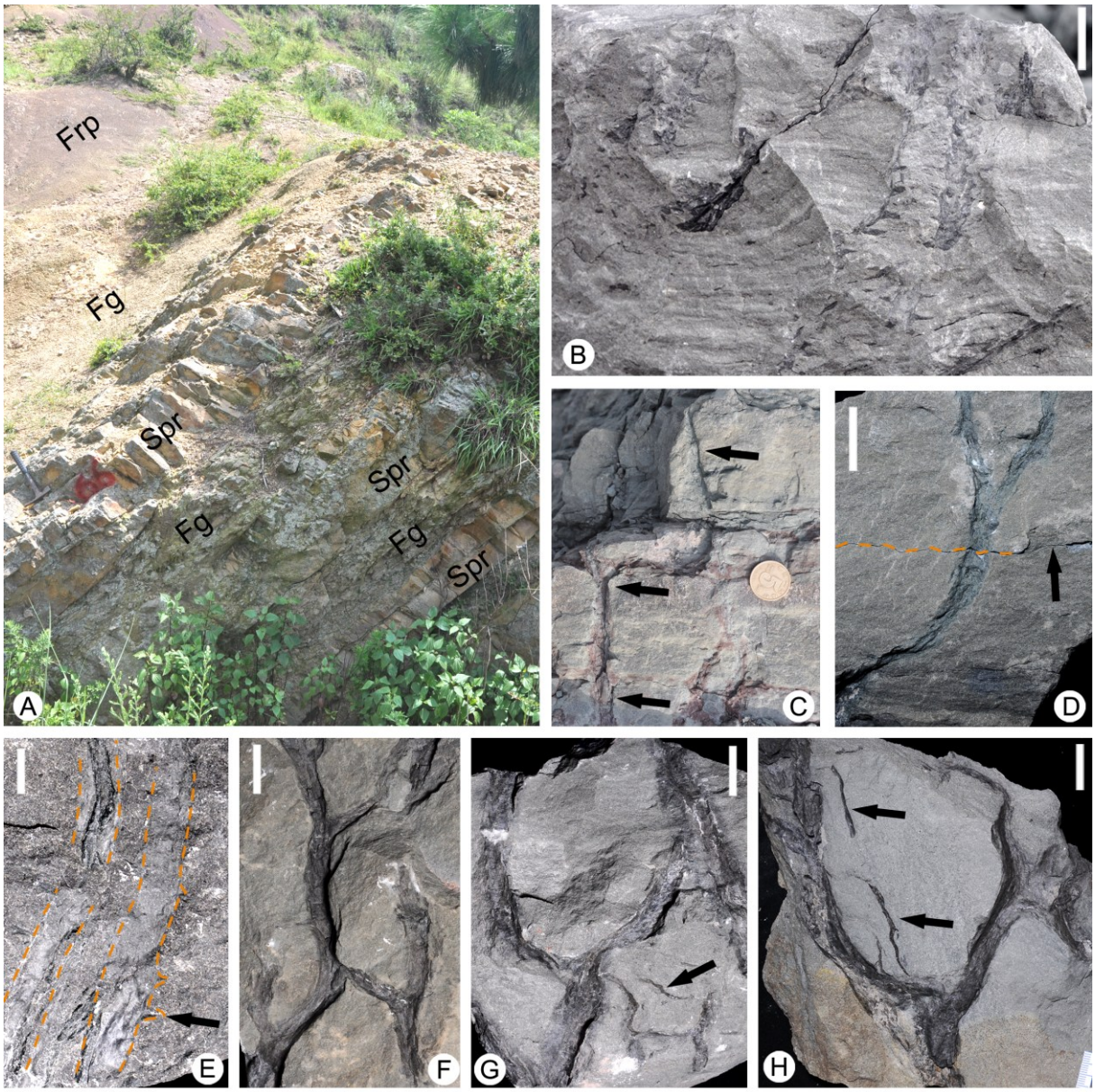

Fig. S5. Field outcrop and plant traces of the Xujiachong Formation. Facies codes: medium to thickly bedded gray sandstone (St); thinly bedded gray-green sandstone (Spr); gray-green mudstone and siltstone (Fg); and red pedified mudstone (Frp). (*A*) Succession from red mudstone to gray-green siltstone (Cycle 67). (*B*) Gray-green siltstone (Cycle 80) truncated by sandstone (Cycle 81). (*C*−*F*) Rocks from the Baojia Tunnel section. (*C*, *D*) Gray siltstone with vertical plant traces. (*E*) Plant traces, continuous and extending vertically from red to gray-green mudstone (arrows). (*F*) Gray siltstone with vertical plant traces (black arrows), which are truncated by thinly bedded sandstone. Note the plant traces bend to become horizontal at the base of the sandstone (white arrow).

Fig. S5.

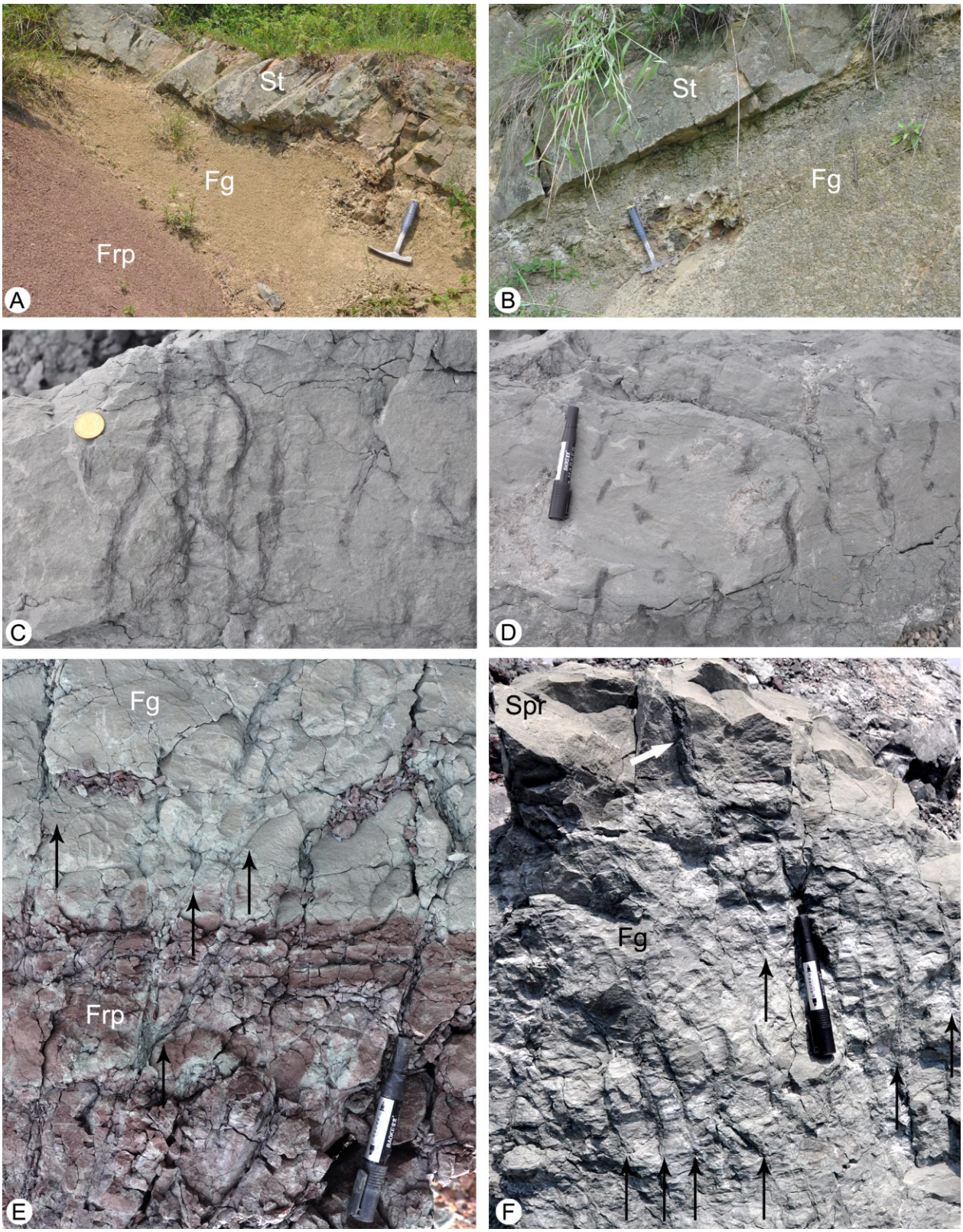

Fig. S6. Specimens with plant remains and traces (gray-green siltstone and mudstone, Facies Fg, from the Baojia Tunnel section). (*A*) Traces on bedding surface. Scale bar, 100 mm. (*B*) Enlarged view of the counterpart of the squared area in (*A*), showing wide rhizome traces with thin, adventitious roots (arrows). Stars, attachment points of roots. Scale bar = 40 mm. (*C*−*H*) Compression remains of leafy aerial axes of *Drepanophycus qujingensis*. (*C*) Two adjacent beds, each with parallel aerial axes indicative of current. Scale bar, 40 mm. (*D*) Axis showing dichotomous branching. Scale bar, 10 mm. (*E*) Dichotomous axis with typical microphylls. Scale bar, 10 mm. (*F*) Dense aerial axes. Scale bar, 30 mm. (*G*) Clearly pseudomonopodial branching of aerial axis with small lateral branches. Scale bar, 10 mm. (*H*) Aerial axis with vestige of vascular strand in the middle. Scale bar, 10 mm.

Fig. S6.

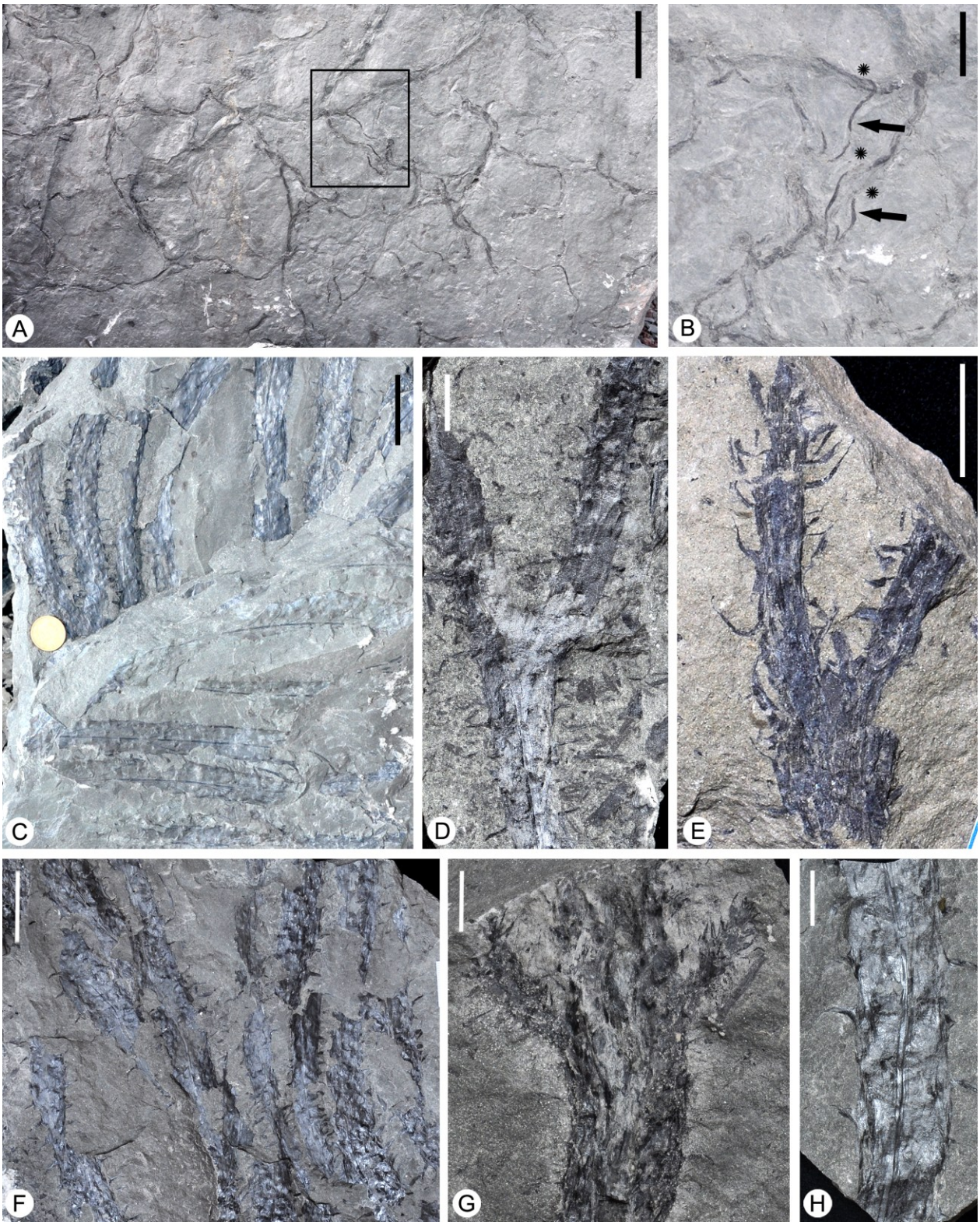

Fig. S7. Field outcrops showing Facies Frp – red mudstone (paleosols) in the Xiaoguankou section. (*A*) Outcrops showing part of a 15.5-m-thick paleosol (lithological column shown in Fig. 2*G*). (*B*) Gray vertical plant traces extensively occurring in red mudstone. Facies codes: thinly bedded gray-green sandstone (Spr); and red pedified mudstone (Frp). (*C*) Gray vertical traces with complex branchings. Ruler for scale, 100 mm.

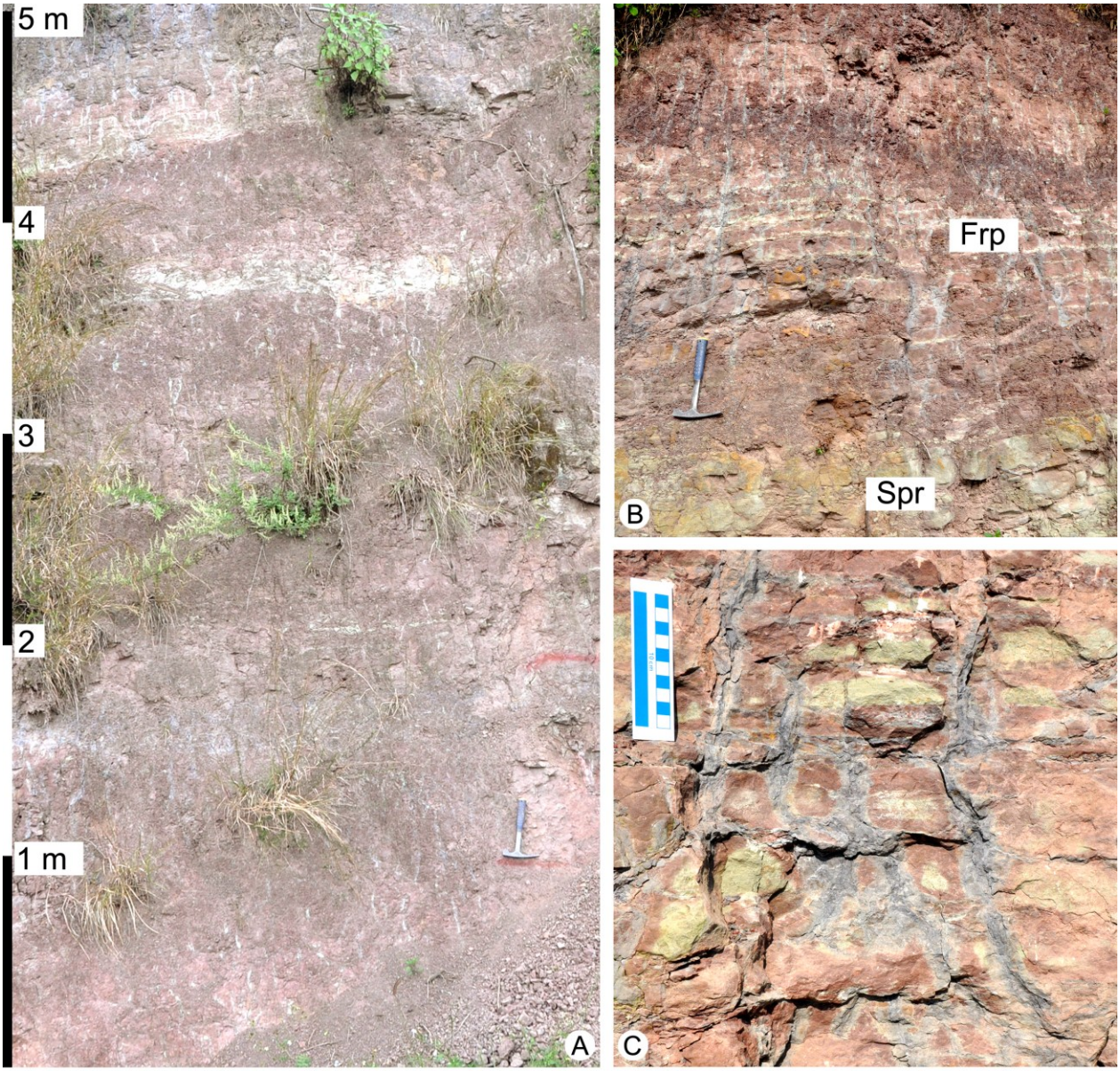

Fig. S8. Facies Frp – red pedified mudstone. (*A*) Outcrop at Xujiachong (Cycle 35; lithological column shown in Fig. 2*C*). (*B*, *C*) Rocks from the Baojia Tunnel section. (*B*) Vertical plant traces. Arrows point to the levels where plant traces become horizontally extended and where branchings are more frequent. (*C*) Bedding surface, showing transections of plant traces (black circles), and horizontally extended traces (arrows). (*D*) Cycle 35 at Xujiachong, transections of plant traces showing as small gray dots, and 12 quadrats (100 mm by 100 mm for each) for estimation of trace density. Scale bar, 100 mm. (*E*) Density map of the plant traces (black dots) shown in (*D*). Hot and cold colors represent high and low density, respectively.

Fig. S8.

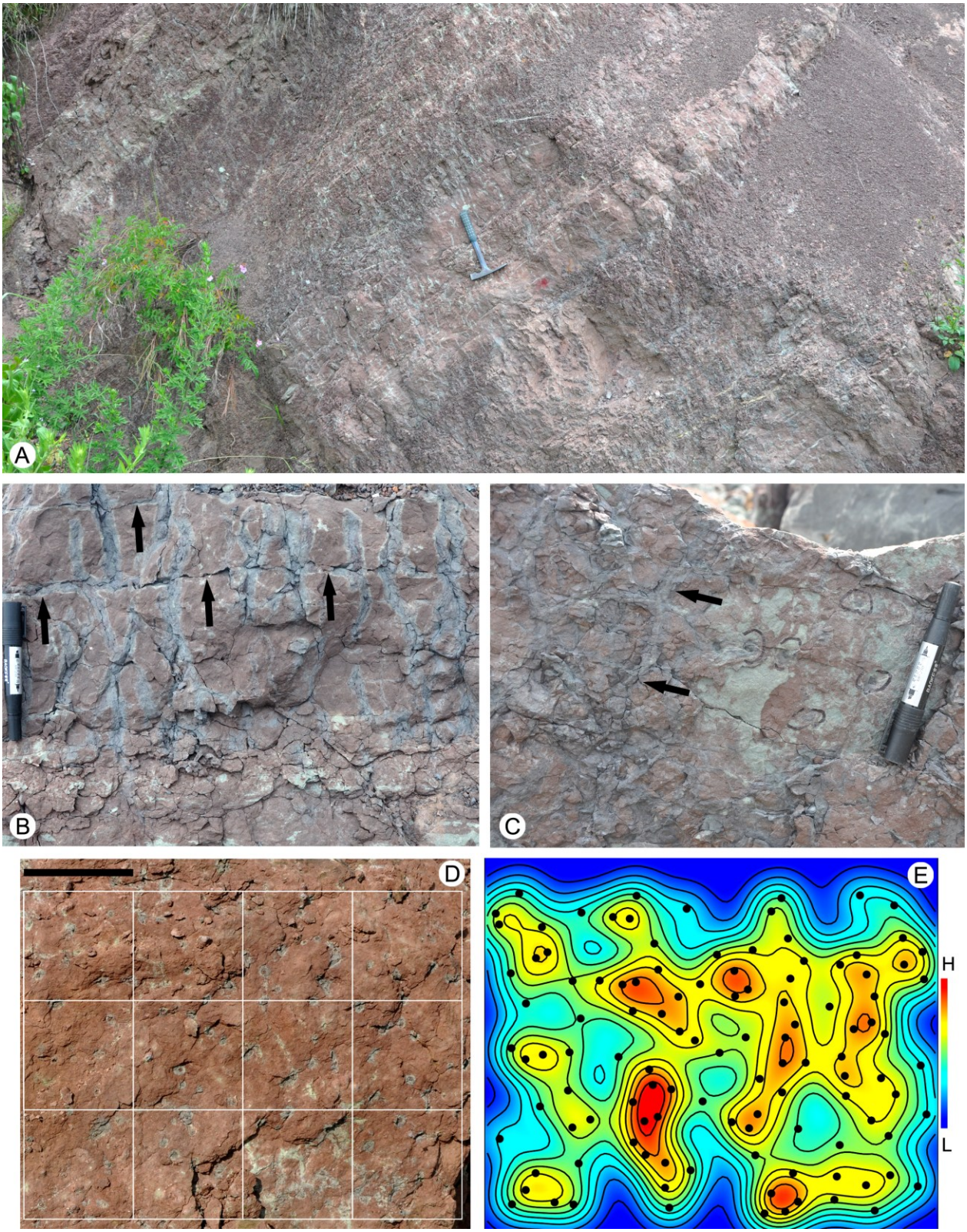

Fig. S9. Facies Frp – red pedified mudstone. (*A*) Red mudstone at Xiaoguankou. Ruler for scale, 100 mm. (*B*) Enlargement of the outcrop, showing the distribution of pedogenic carbonate nodules. Scale bar, 100 mm. (*C*) Red mudstone in Cycle 35 of the Xujiachong section, showing vertical plant traces and scattered carbonate nodules. Scale bar, 100 mm. (*D*) Polished vertical section of red mudstone (sample 148XJC014) from Cycle 35 in the Xujiachong section, showing scattered carbonate nodules of different sizes. Scale bar, 10 mm. (*E*) Thin section of a carbonate nodule within a plant trace (right part, light colored). Left part is the red mudstone matrix (dark colored). Scale bar, 2 mm. (*F*) Polished transverse surface of plant traces. Scale bar, 20 mm.

Fig. S9.

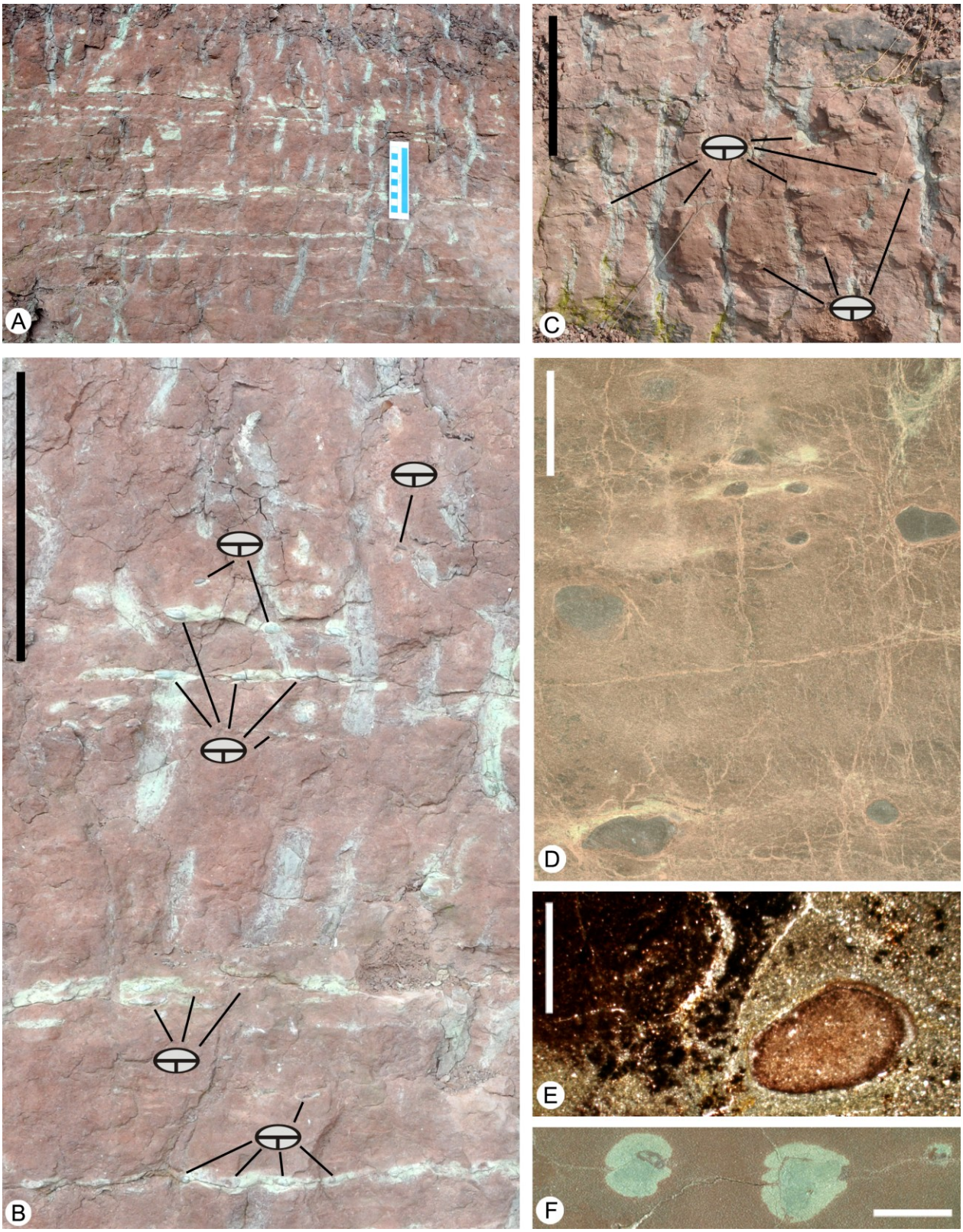

Fig. S10. Serial transverse sections and side view of a rock block (sample 1410XGK37) containing plant rhizome traces. (*A-1*, *A-2*, *A-6*) Three sections with transections of rhizome traces, showing as gray-green dots or horizontal extensions (indicative of K- or H-shaped branching). Sectioned positions shown in (*C*). (*B*−*E*) View of four sides, showing vertically aligned rhizome traces, some with H-shaped branching trace (*B*) and rhizocretions (arrows in *B* and *D*).

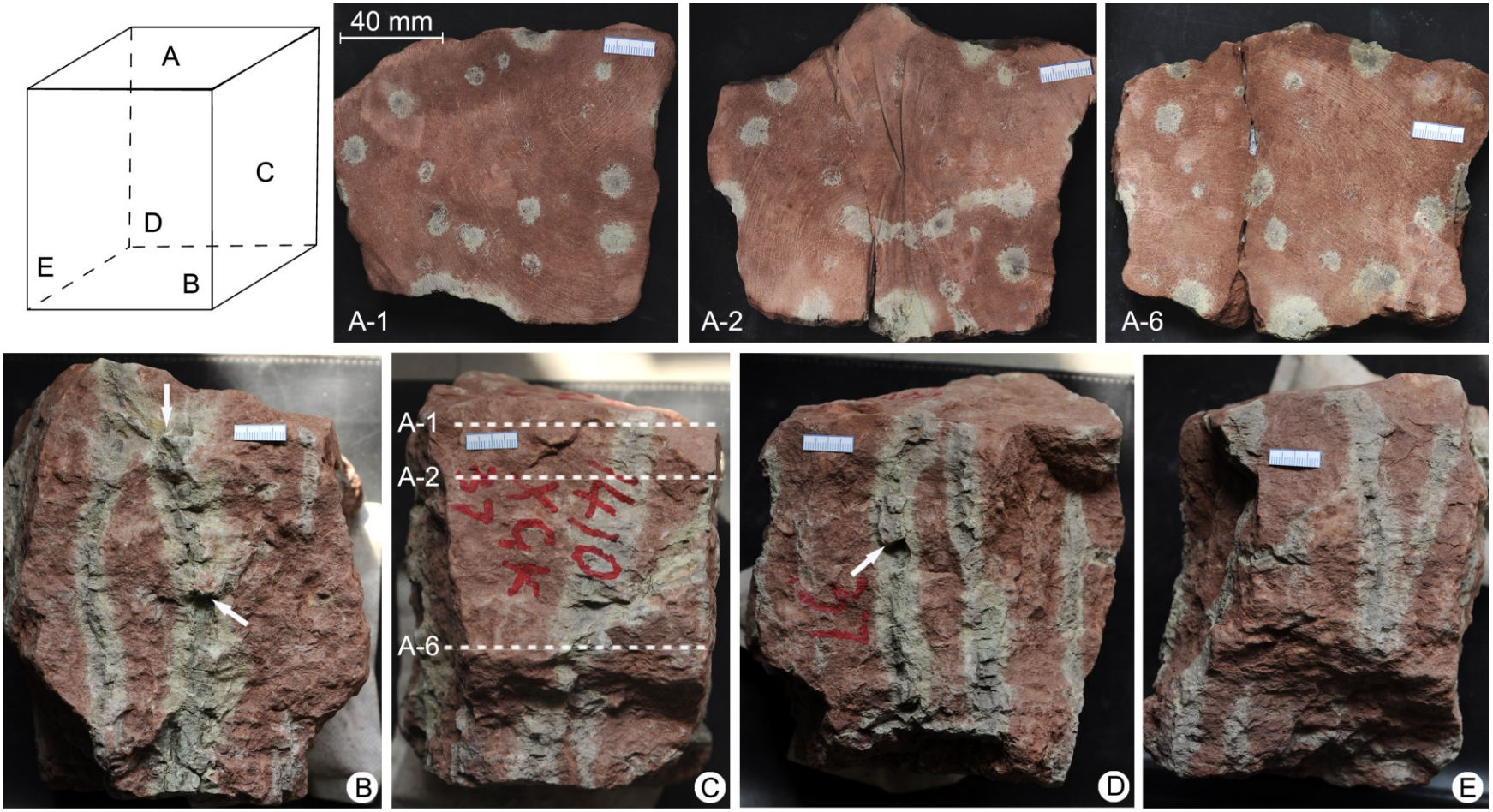

Fig. S11. Representative serial transverse sections of the rock block shown in Fig. S10 (from A-1 to A-8, sequentially with an interval of ca. 2 cm), and three-dimensional reconstruction of the rhizome system. Only the saturation of the original illustrations was adjusted to increase the contrast between rhizome traces and rock matrix. The rhizomes reach ca. 10.1% by volume in the ca. 2000-cm^3 rock block, and the total rhizome length reaches 240 cm (and thus the rhizome length per cubic meter of sediment is 1.2 km).

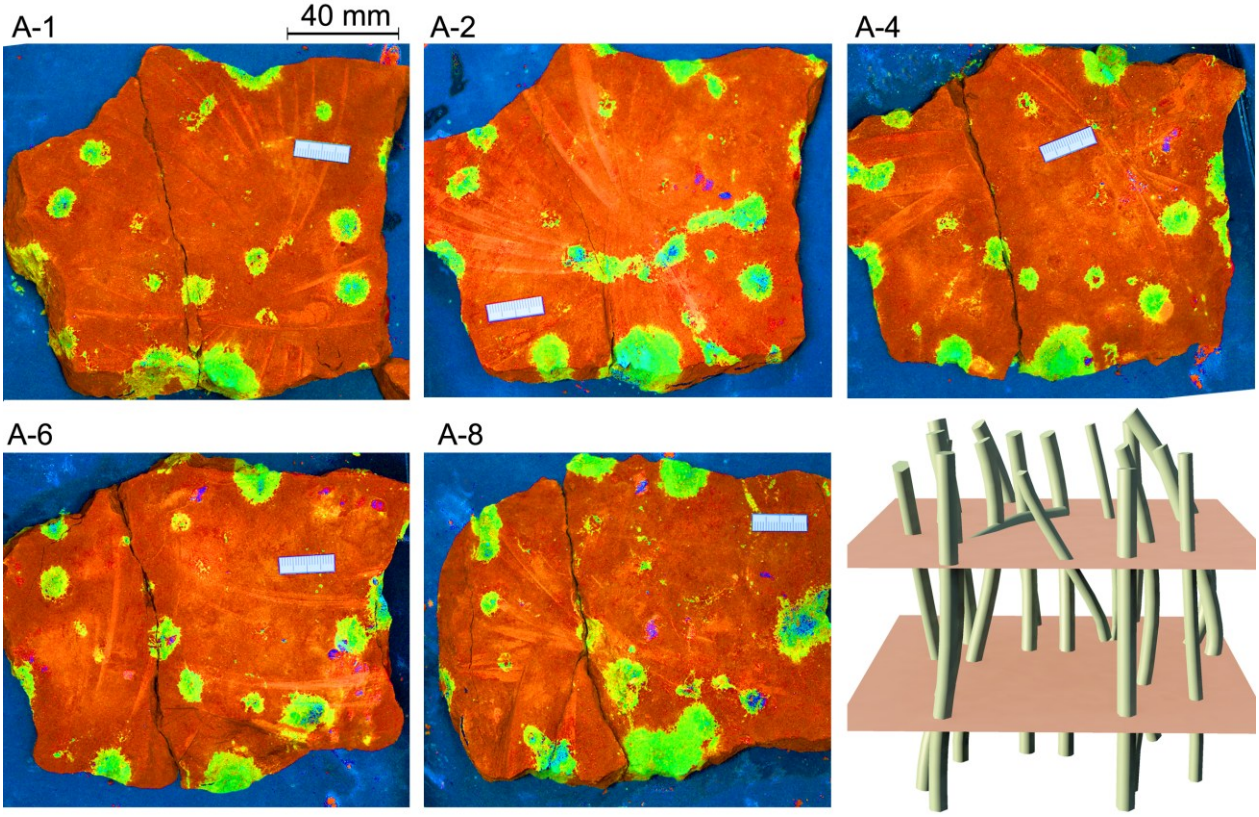

Fig. S12. Plant traces, pedogenic carbonate nodules and their element mapping. (*A*) Polished vertical section of red mudstone, with green plant traces and scattered nodules, from Cycle 35 in the Xujiachong section. Also shown in Fig. 2*E* (upper right part). Square, position for X-ray compositional mapping for Silicon (*B*), Aluminum (*C*), Calcium (*D*), Carbon (*E*), Iron (*F*), and Magnesium (*G*). The relative abundance of the elements, from low to high, is shown by the gradient from cold to hot colors. Scale bars, 2 mm.

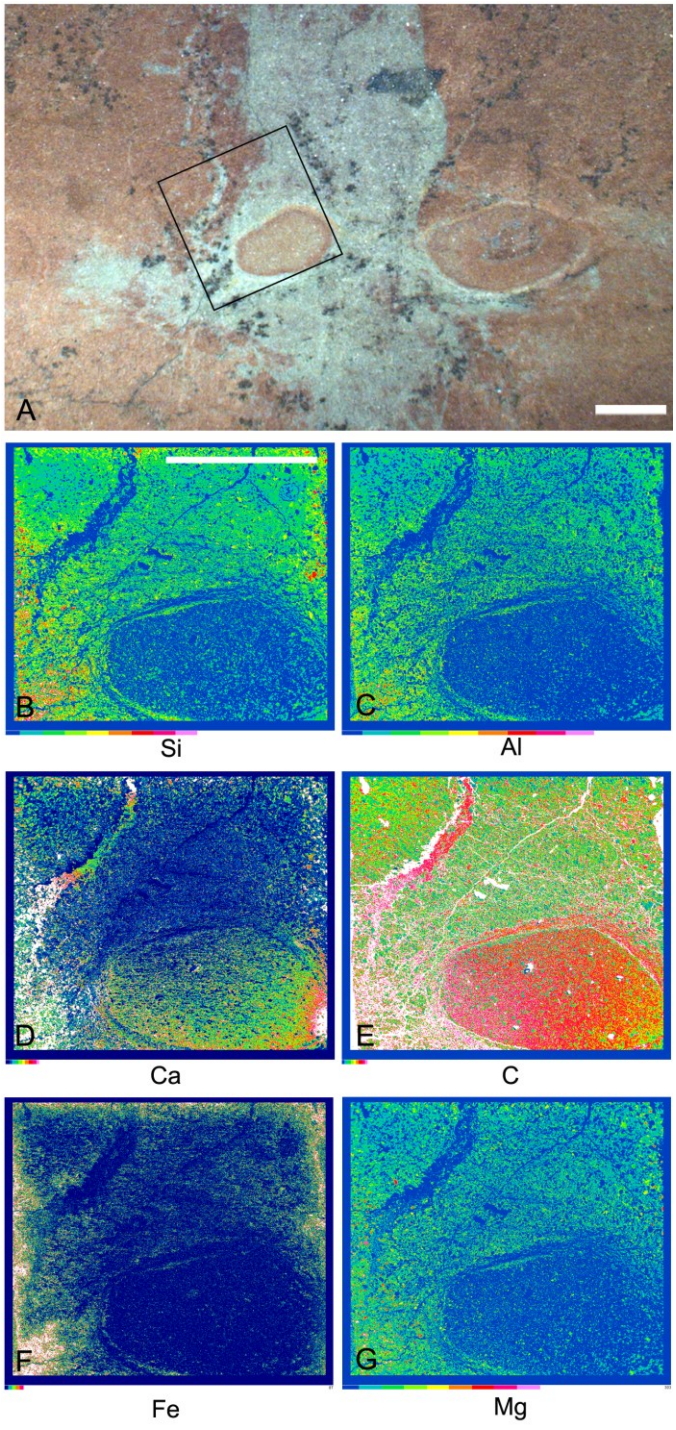

Fig. S13. Interpretative drawings of the rhizome traces preserved in rock blocks (*A* = Fig. 2*I*; *B* = Fig. S8*B*; *C* = Fig. 2*H*). (*A*) Traces on vertical section bend to become horizontal on the upper, horizontal surface. (*B*, *C*) Traces on vertical section, with K- or H-shaped branchings. Arrows point to the levels where branchings appear to be more frequent than at other levels.

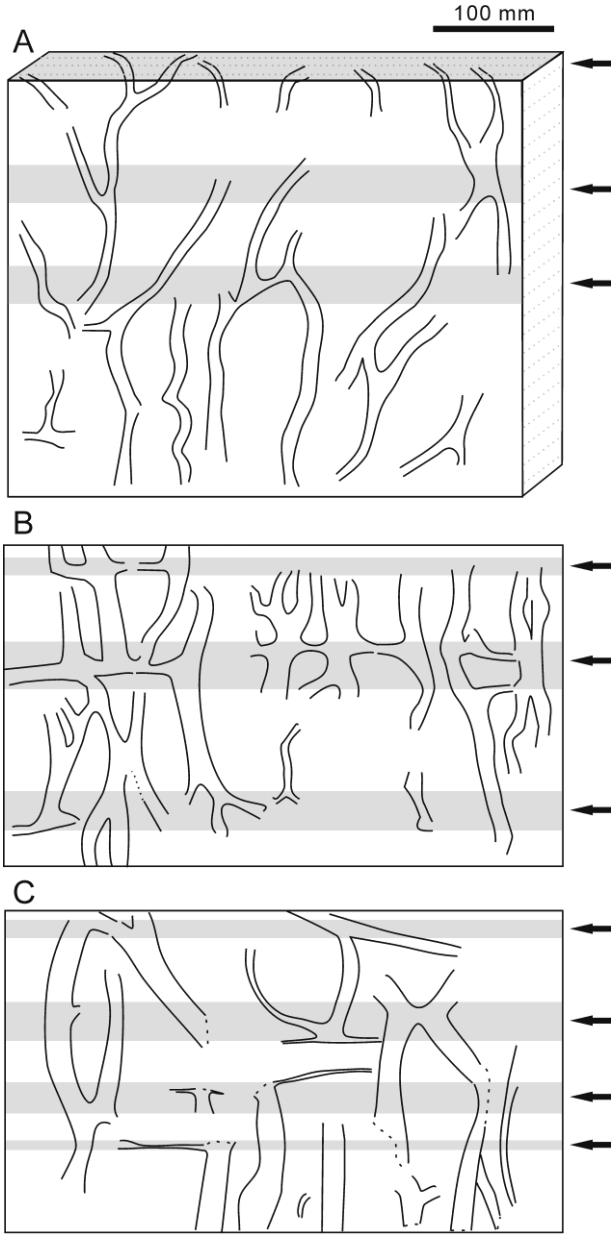

Fig. S14. Box plot for the width of rhizome traces (e.g., Figs. 2*H* and *I*; Fig. S4*F*−*H*) and aerial axes of *Drepanophycus* (e.g., Fig. S6*C*−*H*). Lines in box are median values, boxes are 25−75 percent quartiles, and upper and lower lines are range.

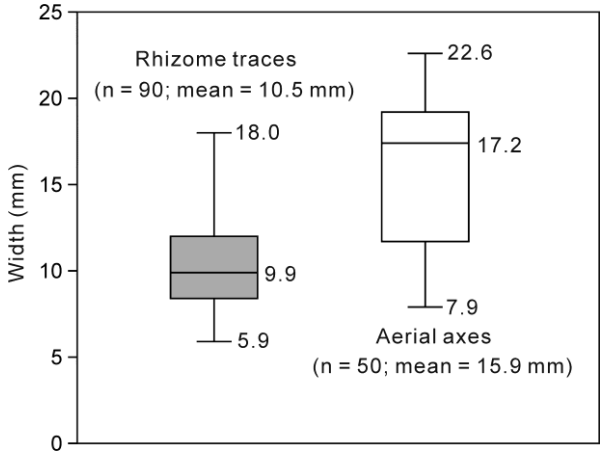

Fig. S15. Histogram showing the size distribution of carbonate nodules occurring in the paleosols of the Xujiachong Formation of Yunnan, China.

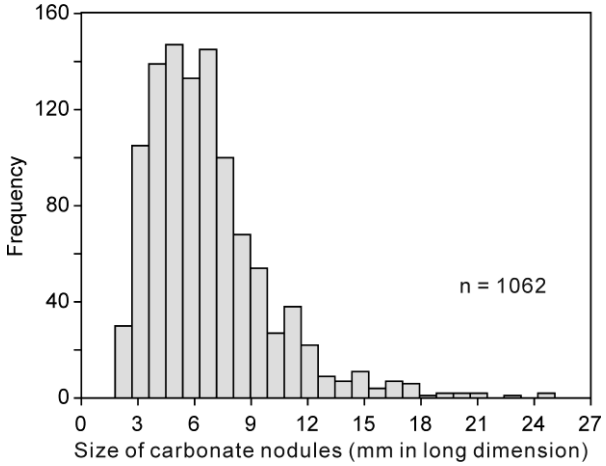

Fig. S16. Geochemical characteristics of the paleosols of the Xujiachong Formation (see text for details; data in Tables S4−S6). (*A*) Cycles 35−37 in the Xujiachong section. (*B*) Cycle 33 in the Xujiachong section. (*C*) The Xiaoguankou section. $\delta^{13}C_{carb}$, stable carbon isotope values of carbonate nodules; $\delta^{13}C_{OM}$, stable carbon isotope values of organic matter within the paleosols; $\Delta 13C_{carb-OM}$, the difference between $\delta^{13}C_{carb}$ and $\delta^{13}C_{OM}$.

Fig. S16.

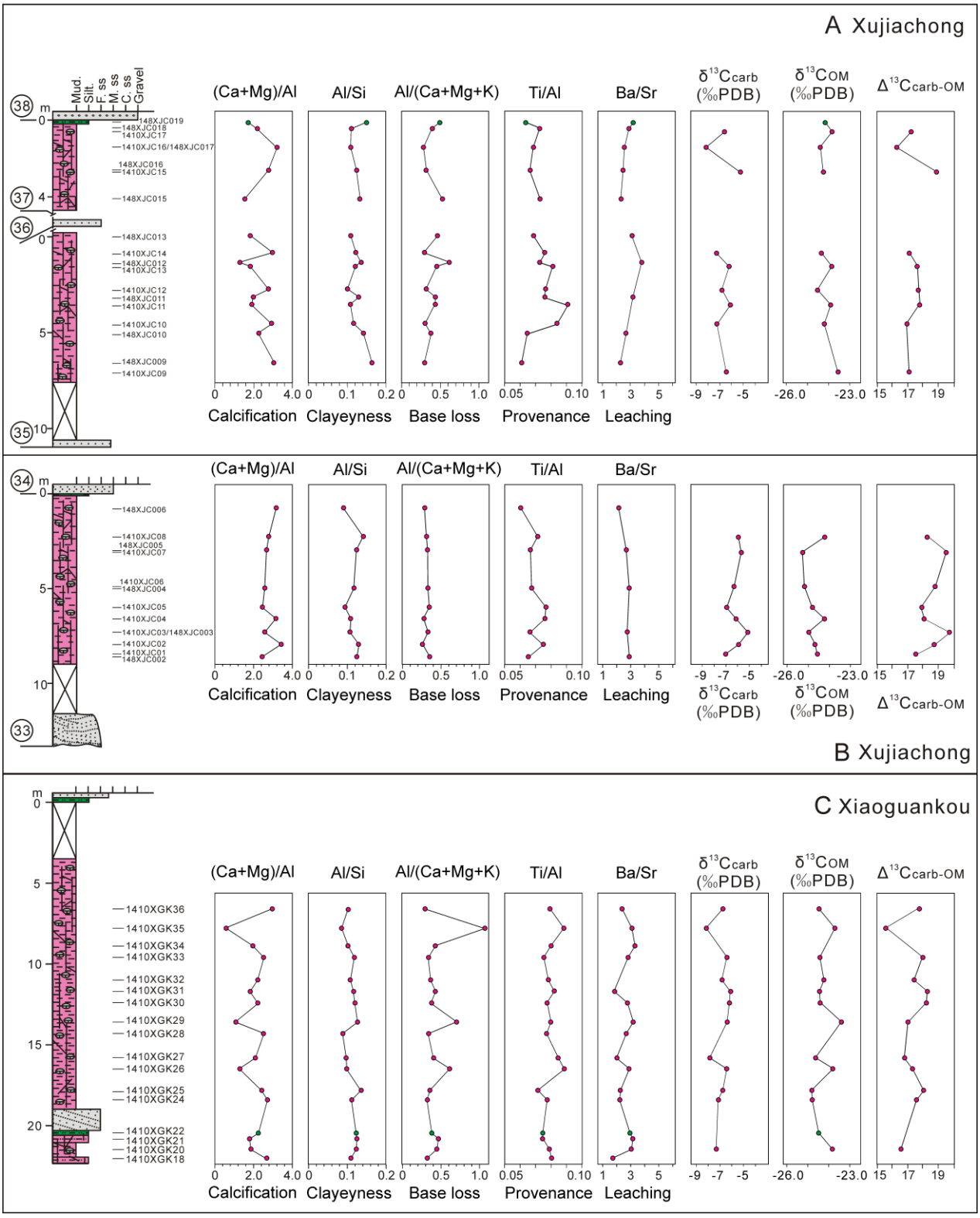
A Xujiachong
B Xujiachong
C Xiaoguankou
Mud.
Silt.
F. ss
M. ss
C. ss
Gravel
m
(Ca+Mg)/Al
Al/Si
Al/(Ca+Mg+K)
Ti/Al
Ba/Sr
δ13Ccarb (‰PDB)
δ13COM (‰PDB)
Δ13Ccarb-OM
Calcification
Clayeyness
Base loss
Provenance
Leaching
148XJC019
148XJC018
1410XJC17
1410XJC16/148XJC017
148XJC016
1410XJC15
148XJC015
148XJC013
1410XJC14
148XJC012
1410XJC13
1410XJC12
148XJC011
1410XJC11
1410XJC10
148XJC010
148XJC009
1410XJC09
148XJC006
1410XJC08
148XJC005
1410XJC07
1410XJC06
148XJC004
1410XJC05
1410XJC04
1410XJC03/148XJC003
1410XJC02
1410XJC01
148XJC002
1410XGK36
1410XGK35
1410XGK34
1410XGK33
1410XGK32
1410XGK31
1410XGK30
1410XGK29
1410XGK28
1410XGK27
1410XGK26
1410XGK25
1410XGK24
1410XGK22
1410XGK21
1410XGK20
1410XGK18

Fig. S17. Chondrite-normalized REE abundances in the samples of the Xujiachong Formation and North American Shale Composite (NASC) (10). Leedey chondrite data based on ref. 11.

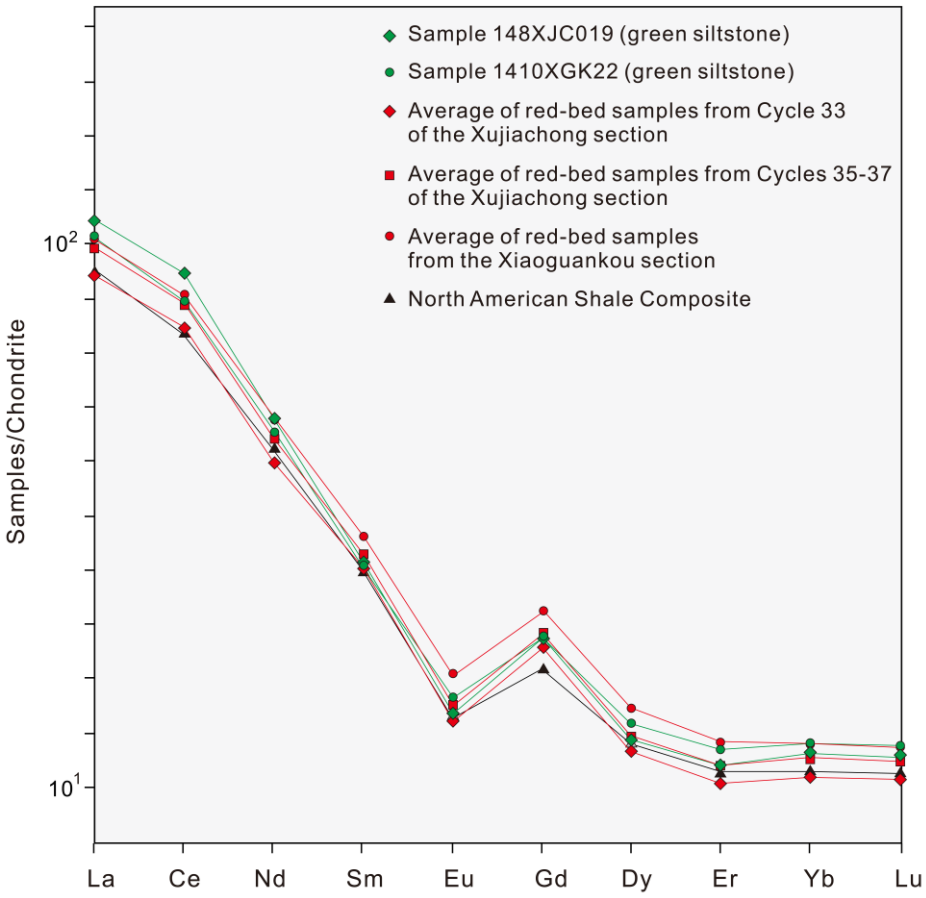

Fig. S18. Cross-plot of stable carbon and oxygen isotope values (*A*) and statistics of the carbon isotopes (*B*) of the carbonate nodules from the paleosols of the Xujiachong Formation of Yunnan, China. Diamonds and crosses in (*A*) indicate samples from the Xujiachong and Xiaoguankou sections, respectively.

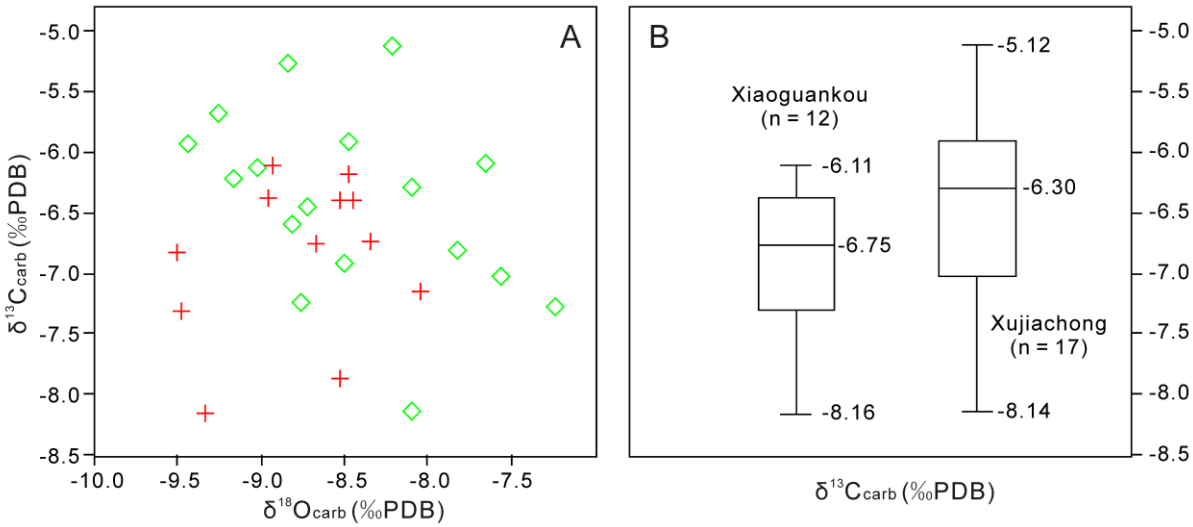

Fig. S19. Artist's reconstruction of an Early Devonian river landscape, with the plant community dominated by *Drepanophycus*, based on the Xujiachong Formation of Yunnan, China.

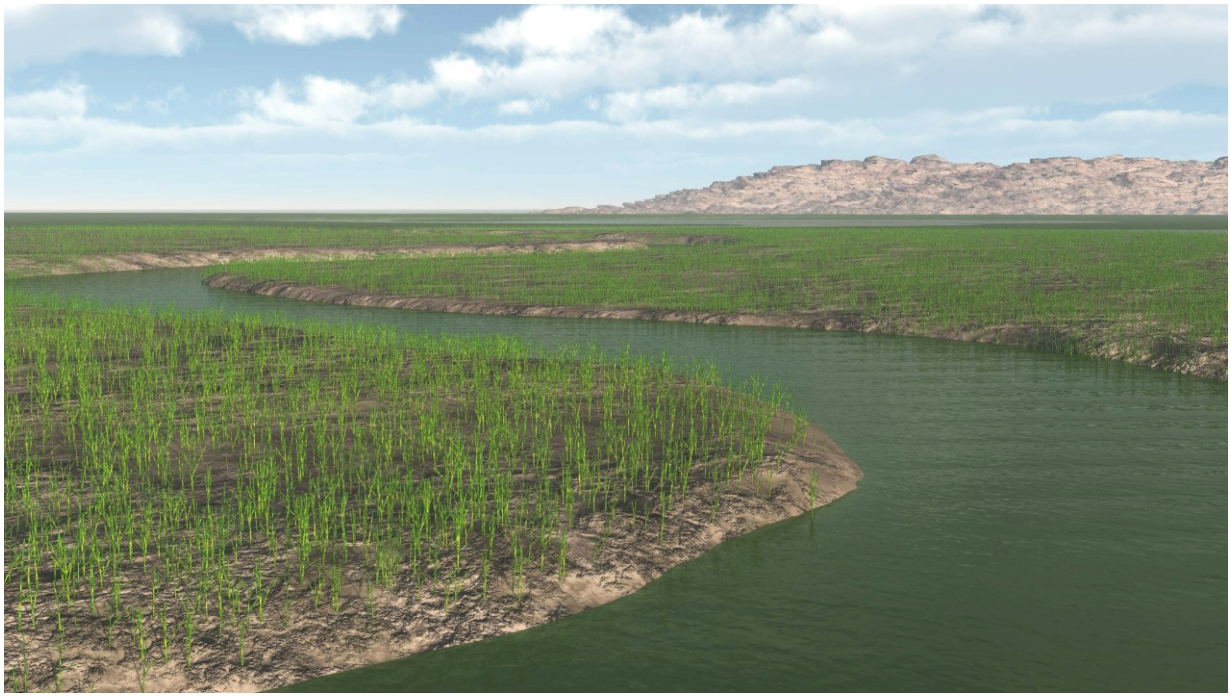

Table S1. Summary of lithologic and sedimentologic features, plant fossils, and interpreted sedimentary environments of the Xujiachong Formation, exposed near Qujing City, Yunnan Province, southwestern China (based on ref. 3 and our re-examination).

Facies	Lithology	Sedimentary characteristics	Thickness of single beds	Sum thickness in the whole section*	Plant fossils	Illustrations	Interpretation
Gt	Gray intraformational conglomerate	Clast- or matrix-supported; moderately to poorly sorted; granules to pebbles; mud or lithic clasts imbricated, subangular to rounded; medium to thickly bedded; planar cross-bedding, fining upward to sandstone (Facies St or Spr); sharp, undulatory bases	Underlying Facies St or Spr, several centimeters	111 m (Facies Gt plus St)	Fragments	Fig. S1	Basal lag of reworked floodplain clasts
St	Medium to thickly bedded gray sandstone	Mainly of fine- to medium-grained, few coarse-grained with granules at base; subarkosic arenite and quartz arenite; poorly to moderately sorted; subangular to subrounded; beds 0.1−1.0 m thick, thinning laterally; channel-form or lenticular in most cases; trough and tabular cross-bedding common; ripple lamination; with lens of gray-green siltstone; sharp, erosional bases; sharp, planar or gradational upper boundaries	0.1−1.0 m, average 0.4 m (n = 32)		Transported fragments and *in situ* remains of *Drepanophycus qujingensis*; Rare vertical plant traces	Figs. S2 and S3	Fluvial channel
Spr	Thinly bedded gray-green sandstone	Fine- to medium-grained; subarkosic arenite, quartz arenite, and wackes; poorly to well sorted; subangular to subrounded; thin beds lenticular or sheetlike; gradational or sharp, planar contact with medium to thickly bedded sandstone (Facies St) at the base; sharp contact with red mudstone (Facies Frp); commonly forming couplets with gray-green mudstone/siltstone (Facies Fg) that bears abundant plant fossils	Less than 0.1 m	301 m (Facies Spr plus Fg): 119 m of couplets of Spr and Fg; 55 m dominated by Spr; and 127 m dominated by Fg	Transported fragments and *in situ* remains of *Drepanophycus qujingensis*; Frequent plant traces	Figs. S2C, and S4 *A*−*E*	Laterally accreted point bars or crevasse splays (usually forming couplets with Facies Fg or intercalated within Facies Fg or Frp)
Fg	Gray-green mudstone and siltstone	Commonly forming couplets with Facies Spr (heterolithic facies), or as single beds between Facies Spr and Facies Frp, 0.1 m to several meters thick; medium to	0.1−7.1 m, average 0.9 m (n = 142)		Abundant plant remains: *Bracteophyton variatum*;	Figs. 2 *I*−*K*, and S5 and S6	Laterally accreted point bars or crevasse splays (forming

		well sorted; subangular to subrounded; abundant coalified plant compressions and plant traces on the bedding surface, and abundant vertical plant traces; with fish and bivalves (the upper part of this formation); massive, or with fine lamination			*Drepanophycus qujingensis*; *Guangnania cuneata*; *Hedeia sinica*; *Huia gracilis*; *Hsüa deflexa*; *Zosterophyllum australianum*; *Zosterophyllum yunnanicum*. Abundant plant traces		couplets with Facies Spr), or pedified floodplain (intercalated within or above Faices Frp)
Frp	Red pedified mudstone	See text for details	0.1−14.3 m, average 2.4 m (n = 149)	355 m	Abundant plant traces	Figs. 2 *E*, *F* and *H*; Figs. S7−S12	Pedified floodplain

∗ Sum of the exposed thickness for different lithofacies in the Xujiachong section. The Xujiachong Formation in this section was divided into 93 sedimentary cycles and was estimated ca. 842 m thick (3); this thickness includes some unexposed or heavily covered beds.

Table S2. Density of plant traces (showing as transections) on bedding surface.

0.1 m × 0.1 m quadrat	Number of traces per quadrat	Number of traces per square meter
1	13	1300
2	12	1200
3	11	1100
4	10	1000
5	10	1000
6	10	1000
7	10	1000
8	8	800
9	10	1000
10	9	900
11	10	1000
12	9	900
13	8	800
14	10	1000
15	10	1000
Average	10	1000 (average for 15 quadrats)

Table S3. Size measurements of carbonate nodules in paleosols from the Xujiachong Formation of Yunnan, China.

Sample number	Stratigraphic depth (m)	Width of nodules in long dimension and statistics (mm)					Numbers of measured nodules
		Maximum	Minimum	Mean	Median	Standard deviation	
Samples from Cycle 37 of the Xujiachong section (Fig. 2*C*)							
1410XJC17	-0.6	14.98	4.57	8.63	8.29	2.43	57
1410XJC16	-1.4	24.57	4.66	11.67	11.46	5.37	24
1410XJC15	-2.7	10.35	4.10	6.67	6.28	1.77	23
Samples from Cycle 35 of the Xujiachong section (Fig. 2*C*)							
1410XJC14	-0.9	19.53	5.45	10.49	9.17	4.03	18
1410XJC13	-1.6	8.66	2.69	5.35	5.43	1.64	19
1410XJC12	-2.8	14.06	3.78	8.03	8.17	2.97	48
1410XJC11	-3.6	14.90	1.87	6.11	5.94	2.27	71
1410XJC10	-4.6	10.44	3.25	5.62	4.92	1.97	19
1410XJC09	-7.1	12.91	2.34	5.81	5.37	2.20	80
Samples from Cycle 33 of the Xujiachong section (Fig. 2*D*)							
1410XJC07	-3.1	7.52	2.01	4.59	4.68	1.28	38
1410XJC06	-4.9	15.73	2.09	6.95	6.48	2.62	109
1410XJC05	-6	25.09	4.42	14.85	14.54	5.51	16
1410XJC04	-6.6	11.22	2.69	6.13	5.96	1.96	51
1410XJC03	-7.3	13.44	1.79	6.51	6.68	2.38	73
1410XJC02	-7.95	17.64	4.23	8.98	8.77	3.40	32
1410XJC01	-8.45	20.83	6.40	12.49	11.83	4.02	15
Samples from Xiaoguankou section (Fig. 2*G*)							
1410XGK36	-6.6	19.29	4.47	10.45	9.55	4.09	20
1410XGK35	-7.8	6.98	1.91	3.43	3.24	1.00	66
1410XGK33	-9.6	11.80	2.93	5.56	5.23	1.71	43
1410XGK32	-11	9.92	2.56	5.45	5.11	1.78	43
1410XGK31	-11.7	12.19	2.62	4.78	4.37	2.25	20
1410XGK30	-12.4	11.80	3.87	6.83	6.46	2.16	27
1410XGK29	-13.6	15.63	2.79	6.78	6.55	2.87	20
1410XGK27	-15.8	9.91	3.02	6.00	6.28	1.64	22
1410XGK26	-16.5	5.57	2.51	3.59	3.62	0.75	29
1410XGK25	-17.8	11.54	3.92	5.95	5.20	1.79	44
1410XGK24	-18.4	9.60	6.19	7.89	8.05	1.40	5
1410XGK20	-21.45	11.81	3.16	7.15	6.94	2.47	30

Table S4. Major elements of paleosols from the Xujiachong Formation, Yunnan, China.

Sample number	Stratigraphic depth (m)	Lithology	SiO_2 %	Al_2O_3 %	Fe_2O_3 %	CaO %	MgO %	K_2O %	Na_2O %	MnO %	TiO_2 %	P_2O_5 %	LOI %	Total %
Samples from Cycle 37 of the Xujiachong section (Fig. 2*C*)														
148XJC019	-0.1	Gray-green siltstone	55.71	14.21	3.68	5.37	5.91	3.78	-	0.065	0.710	0.163	10.28	99.89
148XJC018	-0.4	Red mudstone	59.11	11.07	4.00	6.97	4.66	3.03	-	0.077	0.631	0.135	10.19	99.91
148XJC017	-1.4	Red mudstone	53.84	9.99	4.10	9.02	6.31	2.83	-	0.105	0.537	0.180	12.97	99.92
148XJC016	-2.6	Red mudstone	52.60	11.16	4.23	8.47	6.25	3.34	-	0.101	0.582	0.176	12.98	99.90
148XJC015	-4.1	Red mudstone	57.86	13.13	6.34	3.87	5.40	3.73	-	0.057	0.754	0.172	8.56	99.89
Samples from Cycle 35 of the Xujiachong section (Fig. 2*C*)														
148XJC013	0	Red mudstone	61.15	11.32	4.92	4.89	4.81	3.22	-	0.064	0.610	0.192	8.69	99.89
1410XJC14	-0.9	Red mudstone	50.52	10.54	4.79	10.49	4.94	3.57	-	0.084	0.627	0.167	14.17	99.90
148XJC012	-1.4	Red mudstone	58.78	13.81	6.57	3.22	4.95	3.84	-	0.054	0.787	0.180	7.68	99.89
1410XJC13	-1.6	Red mudstone	57.31	11.69	5.86	5.83	4.36	3.80	-	0.077	0.744	0.177	10.05	99.90
1410XJC12	-2.8	Red mudstone	56.51	9.65	4.41	8.77	4.36	3.19	-	0.084	0.578	0.177	12.19	99.91
148XJC011	-3.2	Red mudstone	55.71	12.27	5.58	6.92	4.71	3.46	-	0.062	0.732	0.162	10.28	99.90
1410XJC11	-3.6	Red mudstone	59.07	10.81	5.89	6.17	3.80	3.50	-	0.064	0.770	0.163	9.64	99.88
1410XJC10	-4.6	Red mudstone	52.00	10.27	5.30	9.36	5.19	3.45	-	0.099	0.675	0.174	13.40	99.91
148XJC010	-5.1	Red mudstone	52.67	12.69	4.82	6.84	6.55	3.61	-	0.076	0.642	0.182	11.80	99.90
148XJC009	-6.6	Red mudstone	44.27	12.34	4.62	12.49	5.99	3.47	-	0.099	0.590	0.137	15.87	99.91
Samples from Cycle 33 of the Xujiachong section (Fig. 2*D*)														
148XJC006	-0.8	Red mudstone	58.50	8.96	3.15	9.67	4.53	2.16	-	0.110	0.423	0.193	12.20	99.92
1410XJC08	-2.3	Red mudstone	47.71	11.49	5.67	10.84	4.99	3.85	-	0.089	0.642	0.155	14.46	99.90
148XJC005	-3	Red mudstone	53.41	11.22	4.73	8.08	6.13	3.17	-	0.084	0.588	0.176	12.30	99.91
148XJC004	-5	Red mudstone	54.90	10.94	4.51	8.09	5.58	3.20	-	0.084	0.579	0.188	11.81	99.91
1410XJC05	-6	Red mudstone	59.62	9.49	4.82	7.23	4.13	3.10	-	0.073	0.570	0.194	10.68	99.91
1410XJC04	-6.6	Red mudstone	52.49	9.62	4.81	10.76	4.40	3.22	-	0.119	0.573	0.205	13.70	99.90
148XJC003	-7.3	Red mudstone	57.08	10.40	4.49	7.73	5.17	2.95	-	0.075	0.541	0.180	11.28	99.91
1410XJC02	-7.95	Red mudstone	46.85	10.38	4.86	12.92	4.87	3.53	-	0.089	0.609	0.154	15.62	99.89
148XJC002	-8.6	Red mudstone	54.63	11.56	4.71	7.41	5.89	3.19	-	0.080	0.591	0.186	11.64	99.91
Samples from the Xiaoguankou section (Fig. 2*G*)														
1410XGK36	-6.6	Red mudstone	55.04	9.53	4.35	9.89	4.14	3.23	-	0.089	0.593	0.191	12.85	99.90
1410XGK35	-7.8	Red mudstone	72.19	10.49	6.53	0.47	2.20	3.16	-	0.047	0.726	0.367	3.72	99.90
1410XGK34	-8.9	Red mudstone	60.38	10.45	5.72	4.89	4.60	3.37	-	0.076	0.655	0.203	9.56	99.90
1410XGK33	-9.6	Red mudstone	53.50	10.71	5.72	8.45	4.62	3.59	-	0.119	0.633	0.228	12.34	99.90
1410XGK32	-11	Red mudstone	57.14	10.52	5.03	6.71	4.89	3.44	-	0.083	0.645	0.183	11.27	99.90
1410XGK31	-11.7	Red mudstone	57.62	11.25	6.06	5.18	5.04	3.49	-	0.075	0.723	0.198	10.26	99.91
1410XGK30	-12.4	Red mudstone	55.03	11.17	5.51	7.41	4.59	3.69	-	0.080	0.678	0.182	11.55	99.89
1410XGK29	-13.6	Red mudstone	61.00	13.13	7.18	2.43	3.87	4.08	-	0.047	0.822	0.195	7.15	99.89
1410XGK28	-14.3	Red mudstone	60.57	9.08	4.71	7.45	3.75	2.94	-	0.091	0.549	0.190	10.59	99.91
1410XGK27	-15.8	Red mudstone	60.75	10.08	4.90	5.83	4.21	3.23	-	0.078	0.668	0.305	9.83	99.88

1410XGK26	-16.5	Red mudstone	65.10	10.88	6.00	3.14	3.33	3.49	-	0.052	0.754	0.198	6.93	99.88
1410XGK25	-17.8	Red mudstone	51.57	11.85	5.50	8.16	5.53	3.30	-	0.087	0.662	0.172	13.06	99.90
1410XGK24	-18.4	Red mudstone	54.33	10.22	5.16	8.30	5.04	3.31	-	0.098	0.620	0.178	12.65	99.91
1410XGK22	-20.45	Gray-green siltstone	55.42	11.59	3.88	7.30	5.07	3.62	-	0.092	0.678	0.187	12.06	99.90
1410XGK21	-20.8	Red mudstone	57.45	12.15	5.30	5.50	4.67	3.58	-	0.076	0.709	0.212	10.26	99.90
1410XGK20	-21.45	Red mudstone	56.35	11.73	6.08	6.54	4.02	3.73	-	0.087	0.724	0.178	10.46	99.89
1410XGK18	-22	Red siltstone	54.70	10.16	5.00	8.46	4.79	3.40	-	0.116	0.639	0.197	12.44	99.90

Note: Analyses were made by sequential X-ray fluorescence (XRF) spectrometer at the Key Laboratory of Orogenic Belts and Crustal Evolution at Peking University. Oxides are in weight percent; Fe_2O_3, total iron; Na_2O%, too low to be detected; LOI, loss on ignition.

Table S5. Trace elements of paleosols from the Xujiachong Formation, Yunnan, China.

Sample number	Sc	Sr	Y	Ba	La	Ce	Pr	Nd	Sm	Eu	Gd	Tb	Dy	Ho	Er	Tm	Yb	Lu
Samples from Cycle 37 of the Xujiachong section (Fig. 2*C*)																		
148XJC019	14	62.5	28.3	317	41.8	86.1	9.34	34	5.95	1.18	5.85	0.84	4.76	0.97	2.79	0.44	2.87	0.44
148XJC018	10.9	57.9	28.5	266	36.7	73.7	8.2	30.7	6.08	1.24	5.95	0.86	4.87	0.99	2.85	0.44	2.89	0.44
148XJC017	9.4	59.6	27.1	242	34.2	72.2	8.18	31.6	6.6	1.27	6.26	0.88	4.9	0.98	2.72	0.42	2.75	0.42
148XJC016	10.7	65.9	26.5	257	34.7	70.2	7.84	28.8	5.78	1.16	5.57	0.81	4.57	0.93	2.65	0.41	2.68	0.41
148XJC015	13.1	86.9	28.5	318	40.8	83.5	9.05	33.1	6.29	1.23	6.03	0.87	4.93	1.01	2.89	0.45	2.9	0.45
Samples from Cycle 35 of the Xujiachong section (Fig. 2*C*)																		
148XJC013	10.8	52.7	27	263	34.3	71.1	7.92	30.2	6.33	1.25	6.01	0.85	4.69	0.94	2.67	0.41	2.69	0.41
148XJC012	13.6	55.5	29.2	331	41.9	85.4	9.41	34.2	6.48	1.26	6.15	0.9	5.12	1.04	2.92	0.45	2.93	0.45
148XJC011	12.1	56.9	26.6	287	36.7	73.2	8.13	30.3	5.65	1.13	5.49	0.79	4.57	0.94	2.68	0.43	2.79	0.43
148XJC010	12.6	66	28.5	278	37.5	76.4	8.31	30.4	5.82	1.14	5.68	0.82	4.74	0.99	2.84	0.45	2.88	0.44
148XJC009	13.1	81.3	30.5	294	38.9	79.4	8.91	33.2	6.45	1.32	6.33	0.91	5.15	1.04	2.92	0.46	2.94	0.44
Samples from Cycle 33 of the Xujiachong section (Fig. 2*D*)																		
148XJC006	7.61	55.7	27	189	27.6	58	6.71	26.5	5.89	1.18	5.73	0.83	4.63	0.93	2.57	0.39	2.5	0.38
148XJC005	10.8	60	26.8	255	33.6	68.5	7.5	27.7	5.53	1.1	5.49	0.82	4.66	0.95	2.67	0.42	2.74	0.42
148XJC004	10.8	59.4	29.8	271	38.6	78	8.36	31.3	6.28	1.26	6.19	0.87	4.88	0.99	2.75	0.42	2.69	0.41
148XJC003	10.1	56.9	24	248	32	66.6	7.24	27.3	5.63	1.1	5.34	0.76	4.28	0.86	2.42	0.38	2.46	0.38
148XJC002	11	59	24.3	269	34.4	70.8	7.76	28.7	5.7	1.09	5.39	0.76	4.29	0.87	2.49	0.39	2.58	0.4
Samples from the Xiaoguankou section (Fig. 2*G*)																		
1410XGK36	10.8	65.8	31.2	248	34.6	71.9	8.5	32.3	6.53	1.4	6.5	0.98	5.48	1.11	3.11	0.46	2.95	0.45
1410XGK35	11.9	59.4	43.5	287	42.9	92.6	11.2	43.6	10.8	2.26	10.8	1.57	8.28	1.58	4.18	0.56	3.44	0.52
1410XGK34	11.7	51.4	25.3	266	34.4	69.4	7.91	28.2	5.49	1.13	5.3	0.81	4.6	0.94	2.71	0.4	2.61	0.4
1410XGK33	12.8	62.6	35.4	278	40.2	86.6	10.4	40.1	8.2	1.72	8.02	1.21	6.58	1.3	3.53	0.52	3.27	0.49
1410XGK31	12.4	99.9	27.1	294	38.8	77.5	8.86	32	5.74	1.17	5.68	0.85	4.91	1.01	2.9	0.45	2.86	0.44
1410XGK30	12.8	67.3	27.8	295	37.9	75.8	8.85	33.6	6.09	1.27	5.93	0.89	5.02	1.03	2.89	0.45	2.91	0.45
1410XGK29	15.7	68.6	26.8	346	43.4	86.1	9.8	35.4	5.95	1.22	5.74	0.86	4.88	1.01	2.92	0.45	2.92	0.45
1410XGK28	10.6	58.4	25.6	247	33	67.3	7.79	29	5.72	1.2	5.57	0.83	4.57	0.92	2.62	0.39	2.5	0.39
1410XGK27	11.9	86.1	34.3	276	36.3	74.7	8.89	34.2	7.11	1.49	7.17	1.07	5.99	1.22	3.4	0.51	3.27	0.5
1410XGK26	13.7	67.3	28.5	303	40.6	81.6	9.32	34.1	6.09	1.3	6	0.9	5.05	1.05	3	0.46	2.97	0.45
1410XGK25	13	85.3	28.3	302	39.6	79.4	9.17	34.1	6.31	1.31	6.16	0.91	5.1	1.04	2.94	0.45	2.89	0.44
1410XGK24	11.9	76.9	27	267	35.6	71.2	8.31	31.1	5.86	1.24	5.74	0.88	4.93	1.02	2.89	0.45	2.91	0.45
1410XGK22	13.4	66.6	27.6	307	38.8	76.6	8.66	32.5	5.83	1.26	5.84	0.9	5.1	1.05	2.99	0.46	2.99	0.46
1410XGK21	13.5	62.3	27.5	310	42.5	86	9.81	36.7	6.23	1.32	5.99	0.91	5.04	1.04	2.97	0.48	3.1	0.48
1410XGK20	12.5	67.7	30.9	325	40.6	82.6	9.78	37.2	6.93	1.44	6.79	1.02	5.66	1.15	3.24	0.5	3.2	0.49
1410XGK18	11.7	105	29.5	282	36.6	75.4	8.95	35.8	6.63	1.39	6.52	1	5.55	1.13	3.16	0.5	3.18	0.49

Note: Measurements were made with ICP-MS at Peking University; unit: ug/g (ppm). See stratigraphic position in Table S4.

Table S6. Stable isotope data for paleosols and carbonate nodules from the Xujiachong Formation, Yunnan, China.

Sample number	Stratigraphic depth (m)	Lithology	Carbonate nodules (micrite)		Organic matter (whole rock)	$\Delta^{13}C_{carb\text{-}OM}$ (‰)
			$\delta^{13}C_{carb}$ (‰PDB)	$\delta^{18}O_{carb}$ (‰PDB)	$\delta^{13}C_{organic\ matter}$ ($\delta^{13}C_{OM}$; ‰PDB)	
Samples from Cycle 37 of the Xujiachong section						
148XJC019	-0.1	Gray-green siltstone	/	/	-24.17	/
1410XJC17	-0.6	Red mudstone with carbonate nodules	-6.598	-8.809	-23.83	17.232
1410XJC16	-1.4	Red mudstone with carbonate nodules	-8.139	-8.098	-24.39	16.251
1410XJC15	-2.7	Red mudstone with carbonate nodules	-5.271	-8.837	-24.25	18.979
Samples from Cycle 35 of the Xujiachong section						
1410XJC14	-0.9	Red mudstone with carbonate nodules	-7.272	-7.241	-24.34	17.068
1410XJC13	-1.6	Red mudstone with carbonate nodules	-6.213	-9.166	-23.85	17.637
1410XJC12	-2.8	Red mudstone with carbonate nodules	-6.818	-7.825	-24.52	17.702
1410XJC11	-3.6	Red mudstone with carbonate nodules	-6.09	-7.649	-23.9	17.81
1410XJC10	-4.6	Red mudstone with carbonate nodules	-7.24	-8.763	-24.2	16.96
1410XJC09	-7.1	Red mudstone with carbonate nodules	-6.455	-8.719	-23.55	17.095
Samples from Cycle 33 of the Xujiachong section						
1410XJC08	-2.3	Red mudstone with carbonate nodules	-5.923	-9.44	-24.22	18.297
1410XJC07	-3.1	Red mudstone with carbonate nodules	-5.677	-9.26	-25.28	19.603
1410XJC06	-4.9	Red mudstone with carbonate nodules	-6.297	-8.097	-25.18	18.883
1410XJC05	-6	Red mudstone with carbonate nodules	-6.916	-8.5	-24.82	17.904
1410XJC04	-6.6	Red mudstone with carbonate nodules	-6.127	-9.024	-24.25	18.123
1410XJC03	-7.3	Red mudstone with carbonate nodules	-5.116	-8.212	-24.99	19.874
1410XJC02	-7.95	Red mudstone with carbonate nodules	-5.904	-8.475	-24.68	18.776
1410XJC01	-8.45	Red mudstone with carbonate nodules	-7.025	-7.568	-24.58	17.555
Samples from Xiaoguankou section						
1410XGK36	-6.6	Red mudstone with carbonate nodules	-6.738	-8.347	-24.45	17.712
1410XGK35	-7.8	Red mudstone with carbonate nodules	-8.163	-9.34	-23.69	15.527
1410XGK33	-9.6	Red mudstone with carbonate nodules	-6.399	-8.525	-24.41	18.011
1410XGK32	-11	Red mudstone with carbonate nodules	-6.827	-9.51	-24.21	17.383
1410XGK31	-11.7	Red mudstone with carbonate nodules	-6.107	-8.933	-24.43	18.323
1410XGK30	-12.4	Red mudstone with carbonate nodules	-6.178	-8.471	-24.39	18.212
1410XGK29	-13.6	Red mudstone with carbonate nodules	-6.373	-8.962	-23.38	17.007
1410XGK27	-15.8	Red mudstone with carbonate nodules	-7.863	-8.533	-24.63	16.767
1410XGK26	-16.5	Red mudstone with carbonate nodules	-6.405	-8.444	-23.77	17.365
1410XGK25	-17.8	Red mudstone with carbonate nodules	-6.763	-8.672	-24.79	18.027

1410XGK24	-18.4	Red mudstone with carbonate nodules	-7.16	-8.038	-24.77	17.61
1410XGK22	-20.45	Gray-green siltstone	/	/	-24.46	/
1410XGK20	-21.45	Red mudstone with carbonate nodules	-7.306	-9.475	-23.82	16.514
Average for all samples			-6.599	-8.584	-24.324	17.731

Note: $\delta^{13}C_{carb}$, stable carbon isotope values of carbonate nodules; $\delta^{13}C_{OM}$, stable carbon isotope values of organic matter within the paleosol; $\Delta 13C_{carb-OM}$, the difference between $\delta^{13}C_{carb}$ and $\delta^{13}C_{OM}$. All data are presented in standard per mil (‰) notation relative to Vienna Pee Dee Belemnite (V-PDB).

Table S7. Approximate estimation of volume percentage of plant rhizomes (preserved as traces) within the paleosols of the Xujiachong Formation of Yunnan, China.

Parameter	Description	Value
D	Diameter of traces (rhizomes) (mm)	Average 10.5 mm
n	Number of trace transections per square meter on a bedding surface	Minimum 800; Average 1000; Maximum 1300 (see Table S2)
P*	Rhizome volume within per cubic meter of sediments	Minimum 6.9%; Average 8.7%; Maximum 11.3%

Note: The number of rhizome trace transections per square meter on a bedding surface ranges from 800 to 1300 (average 1000; Table S2), and therefore we assume that the length of traces per cubic meter of sediments would be 800 m to 1300 m (average 1000 m), if not considering their horizontal K- or H-shaped branchings.

* Approximate estimation: $P = n \times \pi ([D \times 10^{-3}]/2)^2 \times 100$.

Table S8. Estimation of mechanical effects of *Drepanophycus* rhizomes on soil detachment ratios (SDR), based on material from the Xujiachong Formation of Yunnan, China.

<table>
<tr><td>Parameter</td><td>Description</td><td colspan="2">Value</td></tr>
<tr><td>RLD</td><td>Root length density (rhizome length density in Drepanophycus; unit: km/m^3)</td><td colspan="2">Minimum: 0.8 km/m^3; maximum: 1.3 km/m^3 (see Tables S2 and S7 note)</td></tr>
<tr><td>SDR*</td><td>Soil detachment ratio:
SDR = RLD^{-b}/(c + RLD^{-b})*</td><td>SDR for tap and fibrous root systems
<table>
<tr><th>SDR</th><th>RLD (km/m^3)</th><th>b</th><th>c</th></tr>
<tr><td>0.66</td><td>0.8</td><td>0.46</td><td>0.56</td></tr>
<tr><td>0.61</td><td>1.3</td><td>0.46</td><td>0.56</td></tr>
</table>
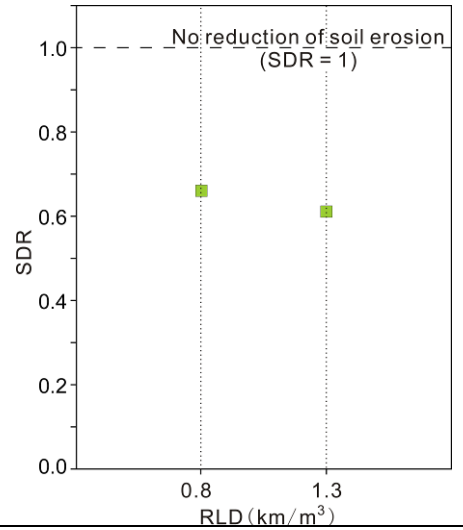
</td><td>SDR for fibrous root systems and non-sandy soil
<table>
<tr><th>SDR</th><th>RLD (km/m^3)</th><th>b</th><th>c</th></tr>
<tr><td>0.86</td><td>0.8</td><td>0.94</td><td>0.20</td></tr>
<tr><td>0.80</td><td>1.3</td><td>0.94</td><td>0.20</td></tr>
</table>
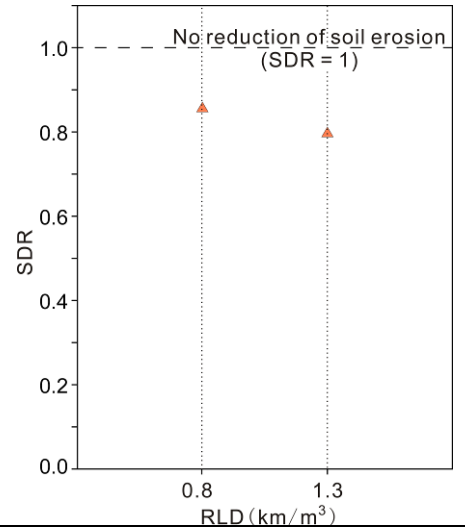
</td></tr>
</table>

* For detailed interpretation of SDR, RLD, and the non-linear regression function, see *SI Appendix*, Quantifying the erosion-reducing potential of *Drepanophycus* rhizomes. Based on Vannoppen et al. (9), the parameters b and c are 0.46 and 0.56, respectively, for the regression fit of 274 observations of modern plant roots including both tap and fibrous root systems, while these two parameters are 0.94 and 0.20, respectively, for the regression fit of 109 observations of fibrous roots in non-sandy soils.

Table S9. Size and lifespan of analogous extant species with clonal growth habit, as a comparison to basal lycopsid *Drepanophycus* from the Xujiachong Formation of Yunnan, China.

Reference plants	Size of clone (diameter, m)	Maximum size of patches	Annual growth rate (mm per year)	Estimated age of oldest clone (years)	Reference
Lycopodium annotinum	Up to 250	-	-	250	(12)
Lycopodium annotinum	36	18,000 m^2	200	150–180	(13)
Lycopodium complanatum	250	-	-	850	(12)
Pteridium aquilinum	489	-	-	1400	(12)
Pteridium aquilinum	> 1015 m across	-	430	1180	(14)

References

1. Li CS, Edwards D (1995) A reinvestigation of Halle's *Drepanophycus spinaeformis* Göpp. from the Lower Devonian of Yunnan Province, Southern China. *Bot J Linn Soc* 118: 163–192.
2. Wang DM, Hao SG, Liu ZF (2002) Researches on plants from the Lower Devonian Xujiachong Formation in the Qujing district, eastern Yunnan. *Acta Geol Sin-Engl* 76: 393–407.
3. Liu ZF, Hao SG, Wang DM, Liu JB (2004) Study on the Xujiachong Formation section of non-marine Lower Devonian of eastern Yunnan, China. *Professional Papers of Stratigraphy and Palaeontology 28*, 61–88, ed. Chinese Academy of Geological Sciences (Geological Publishing House, Beijing).
4. Rohlf FJ (2004) *tpsDig, digitize landmarks and outlines, ver. 2.0* (Department of Ecology and Evolution, State University of New York at Stony Brook [computer program and documentation]).
5. Hammer Ø, Harper DAT, Ryan PD (2001) PAST: Paleontological Statistics Software Package for education and data analysis. *Palaeontol Electron* 4: 9.
6. Gensel PG, Kotyk, ME, Basinger JF (2001) Morphology of above- and below-ground structures in Early Devonian (Pragian–Emsian) plants. *Plants Invade the Land: Evolutionary and Environmental Perspectives*, 83–102, eds Gensel PG, Edwards D (Columbia University Press, New York).
7. Schweitzer HJ (1980) Uber *Drepanophycus spinaeformis* Göppert. *Bonner Paläobotanische Mitteilungen* 7: 1–29.
8. Rayner RJ (1984) New finds of *Drepanophycus spinaeformis* Göppert from the Lower Devonian of Scotland. *Trans R Soc Edinb Earth Sci* 75: 353–363.
9. Vannoppen W et al. (2015) A review of the mechanical effects of plant roots on concentrated flow erosion rates. *Earth-Sci Rev* 150: 666–678.
10. Goldstein SJ, Jacobsen SB (1988) Rare earth elements in river waters. *Earth Planet Sci Lett* 89: 35–47.
11. Masuda A, Nakamura N (1973) Fine structures of mutually normalized rare-earth patterns of chondrites. *Geochim Cosmochim Acta* 37: 239–248.

12. Witte LC, Stöcklin J (2010) Longevity of clonal plants: why it matters and how to measure it. *Ann Bot* 106: 859–870.
13. Wittig R, Jungmann R, Ballach HJ (2007) The extent of clonality in large stands of *Lycopodium annotinum* L. *Flora* 202: 98–105.
14. Parks JC, Werth CR (1993) A study of spatial features of clones in a population of bracken fern, *Pteridium aquilinum* (Dennstaedtiaceae). *Amer J Bot* 80: 537–544.